

# BREAKDOWN OF TORI IN LOW AND HIGH DIMENSIONAL CONSERVATIVE AND DISSIPATIVE STANDARD MAPS

ADRIAN P. BUSTAMANTE, ALESSANDRA CELLETTI, AND C. LHOTKA

**ABSTRACT.** We study the breakdown of rotational invariant tori by implementing three different methods. First, we analyze the domains of analyticity of a torus with given frequency through the computation of the Lindstedt series expansions of the embedding of the torus and the drift term. The Padé and log-Padé approximants provide the shape of the analyticity domains by plotting the poles of the polynomial at the denominator of the Padé approximants. Then, we implement a Newton's method to construct the embedding of the torus; the breakdown threshold is then computed by looking at the blow-up of the Sobolev's norms of the embedding. Finally, according to Greene's method, we estimate the breakdown threshold of an invariant torus with irrational frequency by looking at the stability of the periodic orbits with periods approximating the frequency of the torus.

We apply these methods to 2-dimensional and 4-dimensional standard maps. The 2-dimensional maps can either be conservative (symplectic) or dissipative (precisely, conformally symplectic, namely a dissipative map with the geometric property to transform the symplectic form into a multiple of itself). The 4-dimensional maps are obtained coupling (i) two symplectic standard maps, or (ii) two conformally symplectic standard maps, or (iii) a symplectic and a conformally symplectic standard map. The conformally symplectic maps depend on a dissipative parameter and a drift term, which is needed to get the existence of invariant attractors.

While Padé and Newton's methods perform quite well and provide reliable results, when applying Greene's method, the computation of the periodic orbits in higher dimensional, dissipative maps is particularly complex.

**Keywords.** Symplectic systems, Conformally symplectic systems, Standard map, Invariant tori, Periodic Orbits, Padé approximants, Greene's method, Lindstedt series, Newton's method.

## 1. INTRODUCTION

**1.1. The goal of the work.** As a motivation for studying higher dimensional systems, we consider the example given by the three-body problem (hereafter 3BP) in Celestial Mechanics, which admits different formulations according to the assumptions made. In

---

Corresponding author: *E-mail address:* celletti@mat.uniroma2.it.

A.C. and C.L. acknowledge EU H2020 MSCA ETN Stardust-R Grant Agreement 813644. A.B. and C.L. acknowledge the MIUR Excellence Department Project awarded to the Department of Mathematics, University of Rome Tor Vergata, CUP E83C18000100006. C.L. acknowledges the project MIUR-PRIN 20178CJA2B "New Frontiers of Celestial Mechanics: theory and Applications" and GNFM/INdAM.

the lower dimensional case, the three bodies are subject only to their mutual gravitational attraction, the mass of one body is negligible with respect to that of the other two bodies, the motion takes place on a plane, the orbits of the two primaries are circles around their common barycenter. This model is known as the planar, circular, restricted three-body problem and it can be described by a Hamiltonian system with two degrees of freedom (hereafter, 2 DOF). As a consequence, the phase space is four dimensional (hereafter, 4-dim) and the constant energy surfaces are 3-dim; since invariant tori are 2-dim, they separate the constant energy 3-dim space into invariant regions, thus providing a strong stability property, meaning that invariant tori confine the motion and separate the constant energy phase space into invariant regions. Taking a surface of section on a given energy level, one is led to define a 2-dim map ([31]).

Releasing one or more assumptions that characterize the above 3BP, one is led to a higher dimensional dynamical system, which is typically more interesting from the physical point of view, although more complex. For example, one could consider that the orbits of the primaries are elliptic, instead of being circular. The corresponding planar, elliptic, restricted three-body problem is described in terms of a Hamiltonian system with three DOF ([16], [22]). In this case, the phase space has dimension 6, the constant energy surfaces have dimension 5, but the 3-dim invariant tori do not yield anymore confinement properties, since the orbits can leak through the invariant tori, a well-studied phenomenon known as *Arnold diffusion* ([1]). Taking a surface of section on a given energy level, one obtains a 4-dim map. It is worth mentioning that dissipative effects in Celestial Mechanics are found at different levels; we just quote Poynting-Robertson drag on small particles, the effect of the atmosphere on Earth's satellites, tidal torques on planetary satellites. Such effects greatly contribute to shaping the dynamics of objects in the solar system.

Given this physical motivation, the breakdown of invariant tori in conservative and dissipative 4-dim maps is the core subject of the current work; the 2-dim maps will provide us with relevant information on methods and procedures. Before proceeding, let us specify what we mean by breakdown of invariant tori. The symplectic maps we are going to study can be thought as associated to a nearly-integrable Hamiltonian system (like the restricted 3BP) and they depend on a perturbing parameter, say  $\varepsilon$  (representing the mass ratio of the primaries in the 3BP), such that the map is integrable when  $\varepsilon = 0$  (the Keplerian problem) and it is non-integrable when  $\varepsilon \neq 0$ . An invariant torus with a fixed irrational frequency (precisely, Diophantine), say  $\omega$ , exists in the integrable case. The torus gets deformed when  $\varepsilon$  is different from zero, losing regularity as  $\varepsilon$  increases,

until a critical value, say  $\varepsilon_c$ , is reached at which the invariant torus breaks down. We will implement different methods to compute  $\varepsilon_c$ . An analogous scenario holds for a dissipative map; in this case, we will aim to compute the value of the parameter at which an invariant attractor, with given frequency, breaks down.

**1.2. Maps and frequencies.** The estimate of the breakdown threshold  $\varepsilon_c$  for different 2-dim and 4-dim maps will be our main goal. We will consider conservative and dissipative maps. In particular, we start from the 2-dim standard map introduced by Chirikov in [18], which is an area-preserving, symplectic map; we study also its dissipative version, obtained adding a dissipative parameter and a drift term. It is clear that, in the dissipative case, one can have at most one invariant torus; hence, the confinement between two invariant tori as in the conservative case is no more possible. We will consider also 4-dim maps by coupling two 2-dim symplectic maps, thus obtaining a 4-dim symplectic map. Next, we consider the coupling of a symplectic and a dissipative 2-dim maps, providing what we call a *mixed* 4-dim map, depending on a dissipative parameter and a 1-dim drift term. Finally, we consider the coupling of two 2-dim dissipative maps, which generate a dissipative 4-dim map, depending on two dissipative parameters and two drift terms. We will also introduce the notion of conformally symplectic maps ([13]), which are dissipative maps with the property that they transform the symplectic form into a multiple of itself.

It is worth mentioning that we will mainly consider the classical standard map with only one harmonic, but we will also provide a few results for maps with two harmonics.

In the 2-dim maps, the 1-dim invariant tori are labeled by a scalar irrational frequency. According to KAM theory ([28], [2], [30]), the irrational frequency must satisfy a Diophantine condition. One can construct rational approximants to the frequency by taking the truncations of the continued fraction expansion of the irrational number. Each rational approximant corresponds to a periodic orbit, that better approximates the invariant torus as the period gets longer. In the 4-dim maps, the 2-dim invariant tori are labeled by a frequency vector with two components; in this case, the construction of the rational approximants is more elaborated, see, e.g., [27], [32], [34], [33]. We will implement the so-called Jacobi-Perron algorithm, which gives an explicit procedure to construct the rational approximants to the 2-dim frequency vector of the 4-dim symplectic, mixed, dissipative standard maps. In the applications, we will consider different cases in which the two components of the frequency vector are far or close to rationals.

**1.3. Computing the breakdown threshold.** Having defined the phase space (2-dim or 4-dim), the maps (conservative, mixed or dissipative), the frequency (irrational or rational), we try to answer the question of the determination of the breakdown threshold of rotational invariant tori by implementing three different techniques and by comparing the corresponding results. In particular, we compute the Padé approximants, we construct the tori by a Newton's method, we implement Greene's technique. Let us briefly detail such methods.

Invariant tori are represented by an embedding function, and also by a drift term in the dissipative case. The embedding and the drift can be expanded in Lindstedt series, namely in powers of the perturbing parameter. The terms of the Lindstedt series can be obtained through recursive formulae as solutions of suitable cohomological equations. We compute them up to a given order and then we determine the Padé approximants of the truncated series as the ratio of two polynomials (see [8], [9] for computations concerning the dissipative 2-dim standard map). The location of the zeros of the polynomial at the denominator provides the analyticity domain of the invariant tori in the complex parameter plane. The shape and size of the analyticity domain strongly depends on the nature of the map and the characteristics of the frequency, which could range from a strong irrational frequency to a frequency close to rationals. We also compute the logarithmic Padé approximants ([21]), which complement the results obtained by computing the Padé approximants.

Besides, we compute also the radii of convergence of the Lindstedt series, which give an estimate of the breakdown threshold of the invariant tori.

The Newton's method allows us to construct an invariant torus through a quadratically convergent procedure. Starting from the invariance equation for the embedding and the drift, it relies on the so-called *automatic reducibility* ([19], [13]), according to which, in the vicinity of an invariant torus, there exists a change of coordinates that transforms the linearization of the invariance equation for the torus into a constant coefficient equation. We implement an explicit algorithm, borrowed from [13], to implement a Newton's method to determine the embedding and the drift. Then, we compute the corresponding Sobolev's norms, which provide us an estimate of the breakdown threshold of a torus with fixed frequency. In fact, as already noticed and implemented in [10], [15] (see also [14], [11]), if the torus exists, the Sobolev's norms increase smoothly with the perturbing parameter; when approaching the critical threshold of the perturbing parameter, the Sobolev's norms blow up. This behavior allows us to determine the critical value of the

perturbing parameter associated to the symplectic and conformally symplectic 2-dim and 4-dim maps.

A technique to determine the critical threshold by looking at the behavior of the approximating periodic orbits was developed in [24], which contains an implementation for the symplectic 2-dim standard map (see [23] for an application to volume-preserving maps). However, this map is very peculiar, since it can be written as the product of two involutions; as a consequence, the periodic orbits can be determined as the fixed points of one of these involutions. Unfortunately, this decomposition into involutions does not happen in the dissipative case, a fact that complicates enormously the determination of the periodic orbits, as already noticed in [15]. Despite this complication, we elaborated a method to determine periodic orbits also in the dissipative case, at the expenses of a big computational effort. Then, we implement Greene's method, which is based on the assumption that the breakdown of an invariant torus occurs, when the nearby periodic orbits, with frequencies given by the rational approximants to the frequency of the torus, change character from stable to unstable. In the cases we investigated, we found that Greene's method requires a lot of computational time than Padé method or Sobolev's criterion.

**1.4. Content of the work.** As we have seen in the previous subsections, by investigating the breakdown of invariant tori, we are faced with different questions:

- (i) the behavior of 2-dim and 4-dim maps;
- (ii) the construction of rational approximants for 1-dim and 2-dim frequencies;
- (iii) the intrinsic difference between conservative, mixed, dissipative maps;
- (iv) the implementation of different methods: Padé, Newton, Greene's techniques.

These questions are analyzed in the following sections, which are organized as follows. In Section 2 we introduce the definitions of symplectic and conformally symplectic systems; in Section 3 we give explicit expressions for the 2-dim and 4-dim maps that we are going to study; in Section 4 we discuss the rational approximation to the irrational frequencies; in Section 5 we give the definition of invariant tori; we provide in Section 6 the Lindstedt series expansions of the hull functions representing the tori and we compute the Padé approximants to study the analyticity domains of the tori; Newton's method to construct the invariant tori is presented in Section 7 together with an application of Sobolev's criterion; the search for periodic orbits approximating the tori is described in

Section 8. We also provide an appendix to recall the construction of the Padé approximants and an appendix to provide some basic formulae for the analysis of the linear stability of periodic orbits.

## 2. SYMPLECTIC AND CONFORMALLY SYMPLECTIC SYSTEMS

We consider a discrete system  $f$  defined on a symplectic manifold  $\mathcal{M} = B \times \mathbb{T}^n$ , where  $B \subseteq \mathbb{R}^n$  is an open, simply connected domain with smooth boundary and  $n \geq 1$  denotes the number of degrees of freedom of the system. We assume that  $\mathcal{M}$  is endowed with a symplectic form  $\Omega$ ; if  $J$  is the matrix representing  $\Omega$  at  $\underline{x}$ , then for any vectors  $\underline{u}, \underline{v} \in \mathbb{R}^n$ , one has

$$\Omega_{\underline{x}}(\underline{u}, \underline{v}) = (\underline{u}, J(\underline{x})\underline{v}) . \quad (1)$$

Symplectic and conformally symplectic maps have specific geometric properties as given by the following definitions.

**Definition 1.** *A diffeomorphism  $f : \mathcal{M} \rightarrow \mathcal{M}$  is symplectic, if it satisfies*

$$f^*\Omega = \Omega , \quad (2)$$

where  $f^*$  denotes the pull-back of  $f$ .

A special class of dissipative systems is that of conformally symplectic systems, which are defined as follows.

**Definition 2.** *A diffeomorphism  $f : \mathcal{M} \rightarrow \mathcal{M}$  is conformally symplectic, if there exists a function  $\lambda : \mathcal{M} \rightarrow \mathbb{R}$  such that*

$$f^*\Omega = \lambda\Omega . \quad (3)$$

It is known (see, e.g., [13]) that for  $n \geq 2$ , any function  $\lambda$  satisfying (3) must be constant. In the following, we will always consider  $\lambda$  constant. Notice that (3) reduces to (2) by setting  $\lambda = 1$ .

The condition (3) is equivalent to

$$\Omega_{f(\underline{x})}(Df(\underline{x})\underline{u}, Df(\underline{x})\underline{v}) = \lambda\Omega_{\underline{x}}(\underline{u}, \underline{v}) , \quad \forall \underline{u}, \underline{v} \in \mathbb{R}^n .$$

Recalling (1), we have

$$(Df(\underline{x})\underline{u}, JDf(\underline{x})\underline{v}) = \lambda (\underline{u}, J(\underline{x})\underline{v}) ,$$

which must be valid for any  $\underline{u}, \underline{v}$ , thus yielding

$$Df(\underline{x})^T J \circ f(\underline{x}) Df(\underline{x}) = \lambda J(\underline{x}) . \quad (4)$$

As remarked in [13], Definition 2 can be generalized to the case in which the phase space can be written as the product of  $j \geq 2$  manifolds, say

$$\mathcal{M} = \mathcal{M}_1 \times \dots \times \mathcal{M}_j$$

with associated symplectic forms  $\Omega_1, \dots, \Omega_j$ , such that  $\Omega = \Omega_1 \otimes \dots \otimes \Omega_j$ . Then, (3) is replaced by the generalized conformally symplectic condition

$$f^*\Omega = \lambda_1\Omega_1 \otimes \dots \otimes \lambda_j\Omega_j \quad (5)$$

with  $\lambda_j$  constants. Motivated by this remark, we introduce the following notion of systems with *mixed* symplectic and conformally symplectic properties; for short, we will refer to them as *mixed systems*.

**Definition 3.** *Let us consider a domain  $\mathcal{M}$  which can be written as  $\mathcal{M} = \mathcal{M}_1 \times \dots \times \mathcal{M}_j$  with  $j \geq 2$  and let  $\Omega_1, \dots, \Omega_j$  be the symplectic forms associated to  $\mathcal{M}_1, \dots, \mathcal{M}_j$ . Let  $f : \mathcal{M} \rightarrow \mathcal{M}$  be a diffeomorphism with conformal factors  $\lambda_1, \dots, \lambda_j$  as in (5). We say that  $f$  represents a mixed system, if there exists an index  $1 \leq k < j$ , such that*

$$\lambda_1, \dots, \lambda_k \neq 1, \quad \lambda_{k+1} = \dots = \lambda_j = 1. \quad (6)$$

In the case of conformally symplectic and mixed systems, we will consider a family of maps  $f_{\underline{\mu}}$ , where  $\underline{\mu} \in \mathbb{R}^n$  is called the *drift vector*. The reason for introducing extra parameters is that in the symplectic case, without the need of parameters, there exist invariant tori with different frequencies, while in the conformally symplectic case one needs to add a drift parameter vector to have the existence of invariant tori. When considering a family of maps  $f_{\underline{\mu}}$ , we say that  $f_{\underline{\mu}}$  is conformally symplectic if

$$f_{\underline{\mu}}^*\Omega = \lambda\Omega$$

as in (3). Similarly, we extend to the family  $f_{\underline{\mu}}$  the Definition 3 of mixed systems, whenever (6) is satisfied. Examples of symplectic, mixed, conformally symplectic maps are given in Section 3.

### 3. STANDARD MAPS

The core topic of this work is the study of 4-dim maps; nevertheless, we find it convenient to start by introducing the 2-dim conservative and dissipative standard maps; afterwards, we will introduce three different 4-dim standard maps, describing a symplectic, mixed and conformally symplectic system.

**3.1. Conservative and dissipative 2-dim standard maps.** The dissipative 2-dim standard map is defined by the discrete set of equations

$$\begin{aligned} y_{n+1} &= \lambda y_n + \mu + \varepsilon V(x_n) \\ x_{n+1} &= x_n + y_{n+1} , \end{aligned} \tag{7}$$

with  $y_n \in \mathbb{R}$ ,  $x_n \in \mathbb{T}$ ,  $\lambda > 0$  is the conformal factor and  $\mu \in \mathbb{R}$  is the drift parameter, while  $V$  is a regular, periodic function. The determinant of the Jacobian of (7) is equal to  $\lambda$ . Hence, when  $\lambda = 1$  and  $\mu = 0$ , one obtains the symplectic standard map ([18]), while for  $\lambda > 0$  and  $\mu \neq 0$ , one obtains the conformally symplectic standard map, which is contractive for  $0 < \lambda < 1$  and expansive for  $\lambda > 1$ .

**3.2. Symplectic 4-dim standard map.** Also known as the Froeschlé map, it is described by the following equations for  $y_n, w_n \in \mathbb{R}$ ,  $x_n, z_n \in \mathbb{T}$ :

$$\begin{aligned} y_{n+1} &= y_n + \varepsilon V_1(x_n, z_n; \gamma) \\ x_{n+1} &= x_n + y_{n+1} \\ w_{n+1} &= w_n + \varepsilon V_2(x_n, z_n; \gamma) \\ z_{n+1} &= z_n + w_{n+1} , \end{aligned} \tag{8}$$

where  $\varepsilon > 0$  is the perturbing parameter,  $\gamma > 0$  is the coupling parameter, the functions  $V_1, V_2$  are periodic functions of  $x_n, z_n$ , with zero average in both arguments. The map is symplectic, since its Jacobian has determinant equal to one. The system (8) is obtained by coupling two symplectic 2-dim standard maps.

If we define a function  $V$  as

$$V(x, z; \gamma) = -\cos x - \cos z - \gamma \cos(x - z) ,$$

then  $V_1$  and  $V_2$  can be obtained as the derivatives of  $V$ :

$$\begin{aligned} V_1(x_n, z_n; \gamma) &= \frac{\partial V}{\partial x}(x_n, z_n; \gamma) = \sin x_n + \gamma \sin(x_n - z_n) , \\ V_2(x_n, z_n; \gamma) &= \frac{\partial V}{\partial z}(x_n, z_n; \gamma) = \sin z_n - \gamma \sin(x_n - z_n) . \end{aligned} \tag{9}$$



**3.3. Generalized conformally symplectic 4-dim standard map.** It is defined by the equations

$$\begin{aligned} y_{n+1} &= \lambda_1 y_n + \mu_1 + \varepsilon V_1(x_n, z_n; \gamma) \\ x_{n+1} &= x_n + y_{n+1} \\ w_{n+1} &= \lambda_2 w_n + \mu_2 + \varepsilon V_2(x_n, z_n; \gamma) \\ z_{n+1} &= z_n + w_{n+1} , \end{aligned} \tag{10}$$

where  $0 < \lambda_1, \lambda_2 < 1$  are the conformal factors and  $\mu_1, \mu_2 \in \mathbb{R}$  are the drift parameters. The functions  $V_1$  and  $V_2$  can be taken, for example, as in (9). The map (10) is generalized conformally symplectic (compare with (5)) with determinant of the Jacobian equal to the product  $\lambda_1 \lambda_2$ . The system (10) is obtained by coupling two conformally symplectic 2-dim standard maps, which are recovered setting  $\gamma = 0$ .

**3.4. Mixed 4-dim standard map.** It is defined by the equations

$$\begin{aligned} y_{n+1} &= \lambda y_n + \mu + \varepsilon V_1(x_n, z_n; \gamma) \\ x_{n+1} &= x_n + y_{n+1} \\ w_{n+1} &= w_n + \varepsilon V_2(x_n, z_n; \gamma) \\ z_{n+1} &= z_n + w_{n+1} , \end{aligned} \tag{11}$$

where  $0 < \lambda < 1$  is the conformal factor and  $\mu \in \mathbb{R}$  is the drift parameter. The functions  $V_1$  and  $V_2$  can be given, for example, the expressions in (9). The map (11) is of mixed type according to Definition 3; the determinant of its Jacobian is equal to  $\lambda$ . For  $\gamma = 0$  the system (11) reduces to two uncoupled maps, the first one - in  $(y, x)$  - being conformally symplectic and the second one - in  $(w, z)$  - being symplectic.

**Remark 4.** *For later use, it is important to mention that the frequency vector  $\underline{\omega} = (\omega_1, \omega_2)$  associated to (8), (10), (11) can be defined as*

$$\omega_1 = \lim_{n \rightarrow \infty} \frac{\tilde{x}_n - \tilde{x}_0}{n} , \quad \omega_2 = \lim_{n \rightarrow \infty} \frac{\tilde{z}_n - \tilde{z}_0}{n} , \tag{12}$$

where  $\tilde{x}_n, \tilde{z}_n$  denote the  $n$ -th iterates of the lift of the map. We can also write (12) as

$$\omega_1 = \lim_{n \rightarrow \infty} \frac{1}{n} \sum_{j=1}^n y_j , \quad \omega_2 = \lim_{n \rightarrow \infty} \frac{1}{n} \sum_{j=1}^n w_j .$$

## 4. DIOPHANTINE VECTORS AND BEST APPROXIMATIONS

In the following sections, we will analyze the domain of analyticity in the parameters and the breakdown of invariant tori associated to the maps introduced in Section 3.

As it is well known, the existence of invariant tori can be proved by KAM theory, provided a condition on the frequency vector, say  $\underline{\omega} \in \mathbb{R}^n$ , is satisfied. Precisely, it is required that  $\underline{\omega}$  satisfies a Diophantine condition, which is introduced as follows for discrete systems, obtained by combining a pair of 2-dimensional standard maps.

**Definition 5.** *The frequency vector  $\underline{\omega} \in \mathbb{R}^n$  is said to satisfy the Diophantine condition, if*

$$|\underline{\omega} \cdot \underline{m}_1 + m_2|^{-1} \leq \nu^{-1} |\underline{m}_1|^\tau, \quad \underline{m}_1 \in \mathbb{Z}^n \setminus \{0\}, \quad m_2 \in \mathbb{Z} \quad (13)$$

for some constants  $0 < \nu \leq 1$ ,  $\tau \geq 1$ .

For  $\tau > n - 1$ , the set of Diophantine vectors has full Lebesgue measure in  $\mathbb{R}^n$ . By defining  $\underline{\omega}_d = (1, \underline{\omega})$  and setting  $\underline{k} = (m_2, \underline{m}_1)$  with  $m_2 \in \mathbb{Z}$ ,  $\underline{m}_1 \in \mathbb{Z}^n \setminus \{0\}$ , then (13) implies

$$|\underline{\omega}_d \cdot \underline{k}|^{-1} \leq \nu^{-1} |\underline{k}|^\tau, \quad \underline{k} \in \mathbb{Z}^n \setminus \{0\}. \quad (14)$$

In a 4-dim map, as those that will be studied in most of the rest of this work, the frequency vector is 2-dim, say

$$\underline{\omega} = (\omega_1, \omega_2)$$

and the extended vector  $\underline{\omega}_d$  becomes

$$\underline{\omega}_d = (1, \omega_1, \omega_2).$$

For the 2-dim maps, the frequency is a scalar and the Diophantine condition (13) is satisfied by the so-called *noble numbers*, which are real numbers with the property that their continued fraction expansion is definitely equal to one. An example is given by the golden ratio  $\varpi = \frac{\sqrt{5}-1}{2}$ , whose continued fraction expansion is composed by all 1's. A sequence of rational approximants to an irrational frequency is obtained taking the successive truncations of the continued fraction expansion. For the golden ratio, the rational approximants are given by the ratios of successive Fibonacci numbers. The extension of the Diophantine condition and of the rational approximations to a 2-dim frequency associated to a 4-dim map is not trivial and requires some notions, which are briefly recalled in Sections 4.1 and 4.2. For further details, we refer to the specialized literature ([27], [26], [32]).

**4.1. PV numbers and frequency vectors.** To construct the frequency vectors that will be studied in the next sections, we introduce as follows the so-called Pisot-Vijayaraghavan numbers.

Let  $\alpha$  be an algebraic number satisfying a polynomial equation of degree 3 with integer coefficients; we assume that  $\alpha$  does not satisfy polynomial equations of lower degree. Let us introduce the frequency vector  $\underline{\omega}_d = (1, \omega_1, \omega_2)$  as

$$\begin{pmatrix} 1 \\ \omega_1 \\ \omega_2 \end{pmatrix} = \begin{pmatrix} 1 & 0 & 0 \\ b_1 & a_{11} & a_{12} \\ b_2 & a_{21} & a_{22} \end{pmatrix} \begin{pmatrix} 1 \\ \alpha \\ \alpha^2 \end{pmatrix}, \quad (15)$$

where the  $2 \times 2$  matrix  $A := (a_{mn})$  is such that  $\det A \neq 0$ , and where  $A$  and the vector  $(b_1, b_2)$  have rational coefficients.

Let us now add the following definition.

**Definition 6.** A Pisot-Vijayaraghavan (hereafter PV) number of order  $k$  is the only root external to the unit circle in the complex plane associated to a monic polynomial of degree  $k$ , namely a polynomial of the form

$$X^k + \beta_{k-1}X^{k-1} + \dots + \beta_2X^2 + \beta_1X + \beta_0 = 0$$

with  $\beta_j \in \mathbb{Z}$ .

The smallest PV-number of degree 2 is the golden ratio  $\varpi = \frac{\sqrt{5}-1}{2}$ . The smallest PV-number of degree 3 is the real solution of the polynomial  $s^3 - s - 1 = 0$ , namely  $s \simeq 1.324717$ . A remarkable property of PV numbers is the following: if  $\alpha$  is a PV-number and  $\gamma$  is an algebraic integer in the field  $\mathbb{Q}(\alpha)$ , then the distance  $\gamma\alpha^k$ ,  $k \in \mathbb{Z}_+$ , to the nearest integer goes to zero at an exponential rate.

Starting from  $s$  and its inverse, let us construct the vector

$$\underline{\omega}_u = (s^{-1}, s - 1) \simeq (0.7549, 0.3247); \quad (16)$$

it generates the extension  $\underline{\omega}_{u,d} = (1, s^{-1}, s - 1)$ , which satisfies (15), being

$$\begin{pmatrix} 1 \\ s^{-1} \\ s - 1 \end{pmatrix} = \begin{pmatrix} -1 & 0 & 0 \\ -1 & 0 & 1 \\ -1 & 1 & 0 \end{pmatrix} \begin{pmatrix} 1 \\ s \\ s^2 \end{pmatrix}.$$

We notice that both components of  $\underline{\omega}_u$  are close to rationals, say  $(3/4, 1/3)$ . For later use, we also consider the following vectors:

$$\underline{\omega}_a = (s^{-1}, s^{-2}) \simeq (0.7549, 0.5698) \quad (17)$$

with, again, both components close to rationals, say  $(3/4, 1/2)$ ,

$$\underline{\omega}_c = (2(s-1) - \frac{s^{-1}}{24}, s-1) \simeq (0.6180, 0.3247) \quad (18)$$

with the first component close to the golden ratio and the second one close to a rational.

**4.2. Best approximants.** Given  $\underline{\omega} = (\omega_1, \omega_2)$ , the sequence  $\{\frac{p_{1,i}}{q_i}, \frac{p_{2,i}}{q_i}\}_{i \geq 0}$  of the best rational approximants to  $\underline{\omega}$  is defined so that

$$\mathcal{N}_{\underline{\omega}}(p_{1,i}, p_{2,i}, q_i) < \mathcal{N}_{\underline{\omega}}(p'_1, p'_2, q') ,$$

where  $q_0 = 1$ ,  $0 \leq p'_1 \leq q'$ ,  $0 \leq p'_2 \leq q'$ ,  $1 \leq q' \leq q_i$  and with

$$\mathcal{N}_{\underline{\omega}}(p_1, p_2, q) := \sup(|q\omega_1 - p_1|, |q\omega_2 - p_2|) .$$

To find the best approximants, one can construct the extension of the Farey trees to more dimensions (see [27]) or rather implement the *Jacobi-Perron algorithm*, described for example in [29], which generalizes the computation of the continued fraction expansion from one to more dimensions. We will rely on the latter approach, that we briefly summarize as follows.

For a 2-dim vector  $\underline{\omega} = (\omega_1, \omega_2)$ , the Jacobi-Perron algorithm allows one to construct the integer sequences  $p_{1,i}$ ,  $p_{2,i}$ ,  $q_i$ , such that  $(p_{1,i}/q_i, p_{2,i}/q_i)$  are rational approximants to  $\underline{\omega}$ . We follow [32] to describe the Jacobi-Perron algorithm for  $d = 2$  as follows.

Consider the map

$$T(x, y) = \left( \frac{y}{x} - a_1, \frac{1}{x} - b_1 \right) ,$$

with

$$a_1 = a_1(x, y) = \left\lfloor \frac{y}{x} \right\rfloor , \quad b_1 = b_1(x, y) = \left\lfloor \frac{1}{x} \right\rfloor ,$$

and  $a_j(x, y) = a_1(T^{j-1}(x, y))$ ,  $b_j(x, y) = b_1(T^{j-1}(x, y))$ . According to [32], the approximants in terms of sequences  $p_{1,n}$ ,  $p_{2,n}$ ,  $q_n$  are defined by the matrix product

$$\begin{pmatrix} p_{1,n-2} & p_{1,n-1} & p_{1,n} \\ p_{2,n-2} & p_{2,n-1} & p_{2,n} \\ q_{n-2} & q_{n-1} & q_n \end{pmatrix} = \prod_{j=1}^n \begin{pmatrix} 0 & 0 & 1 \\ 1 & 0 & a_j \\ 0 & 1 & b_j \end{pmatrix} .$$

We notice that

$$\begin{pmatrix} p_{1,n-1} & p_{1,n} & p_{1,n+1} \\ p_{2,n-1} & p_{2,n} & p_{2,n+1} \\ q_{n-1} & q_n & q_{n+1} \end{pmatrix} = \begin{pmatrix} p_{1,n-2} & p_{1,n-1} & p_{1,n} \\ p_{2,n-2} & p_{2,n-1} & p_{2,n} \\ q_{n-2} & q_{n-1} & q_n \end{pmatrix} \begin{pmatrix} 0 & 0 & 1 \\ 1 & 0 & a_{n+1} \\ 0 & 1 & b_{n+1} \end{pmatrix} .$$

	$n$	$p_{1,n}$	$p_{2,n}$	$q_n$	$ \omega_1 - p_{1,n}/q_n $	$ \omega_2 - p_{2,n}/q_n $
$\underline{\omega}_u$	2	2	1	2	$2.45 \times 10^{-1}$	$1.75 \times 10^{-1}$
	11	200	86	265	$1.60 \times 10^{-4}$	$1.90 \times 10^{-4}$
	14	1432	616	1897	$1.55 \times 10^{-6}$	$5.29 \times 10^{-6}$
	24	396655	170625	525456	$1.91 \times 10^{-9}$	$2.01 \times 10^{-9}$
$\underline{\omega}_a$	2	1	1	1	$2.45 \times 10^{-1}$	$4.30 \times 10^{-1}$
	11	200	151	265	$1.61 \times 10^{-4}$	$2.90 \times 10^{-5}$
	13	616	465	816	$2.43 \times 10^{-5}$	$1.27 \times 10^{-5}$
	24	226030	170625	299426	$3.13 \times 10^{-10}$	$-3.43 \times 10^{-9}$
$\underline{\omega}_c$	2	1	1	2	$1.18 \times 10^{-1}$	$1.75 \times 10^{-1}$
	6	97	51	157	$1.48 \times 10^{-4}$	$1.23 \times 10^{-4}$
	9	550	289	890	$5.15 \times 10^{-6}$	$1.14 \times 10^{-6}$
	13	210289	110496	340283	$7.27 \times 10^{-10}$	$1.90 \times 10^{-9}$

TABLE 1. Approximants of  $\underline{\omega} = (\omega_1, \omega_2)$  by  $p_{1,n}/q_n, p_{2,n}/q_n$  for  $\underline{\omega}_u, \underline{\omega}_a$ , and  $\underline{\omega}_c$  for various orders  $n$ .

Taking only the 3rd column of the matrix product at the  $(n+1)$ -th step, we get the vectorial recursive formula:

$$\begin{pmatrix} p_{1,n+1} \\ p_{2,n+1} \\ q_{n+1} \end{pmatrix} = \begin{pmatrix} p_{1,n-2} \\ p_{2,n-2} \\ q_{n-2} \end{pmatrix} + \begin{pmatrix} p_{1,n-1} \\ p_{2,n-1} \\ q_{n-1} \end{pmatrix} a_{n+1} + \begin{pmatrix} p_{1,n} \\ p_{2,n} \\ q_n \end{pmatrix} b_{n+1}.$$

The recursion can be solved up to order  $n > 0$  using the starting values (that leave the matrix product unchanged):

$$\begin{pmatrix} p_{1,-2} & p_{1,-1} & p_{1,0} \\ p_{2,-2} & p_{2,-1} & p_{2,0} \\ q_{-2} & q_{-1} & q_0 \end{pmatrix} = \begin{pmatrix} 1 & 0 & 0 \\ 0 & 1 & 0 \\ 0 & 0 & 1 \end{pmatrix}.$$

For example, some of the best approximants to the vectors in (16), (17), (18) are provided in Table 1, which shows the convergence of  $|\omega_j - p_{j,n}/q_n|$ ,  $j = 1, 2$ , to zero, as the order  $n$  increases.

## 5. INVARIANT TORI

Having in mind the 2-dim and 4-dim standard maps introduced in Section 3, we give the following definition of invariant KAM tori for a mapping system.

**Definition 7.** Let  $f : \mathcal{M} \rightarrow \mathcal{M}$  be a diffeomorphism defined on the manifold  $\mathcal{M} = B \times \mathbb{T}^n$  with  $B \subseteq \mathbb{R}^n$  an open, simply connected domain with smooth boundary. Let  $\underline{\omega} \in \mathbb{R}^n$  be the frequency vector, satisfying the Diophantine condition (13). A KAM torus with frequency

$\underline{\omega}$  is an invariant torus described by an embedding  $\underline{K} : \mathcal{M} \rightarrow \mathbb{T}^n$  and a drift  $\underline{\mu} \in \mathbb{R}^n$ , such that the following invariance equation is satisfied:

$$\underline{f}_{\underline{\mu}} \circ \underline{K}(\underline{\psi}) = \underline{K}(\underline{\psi} + \underline{\omega}) , \quad \underline{\psi} \in \mathbb{T}^n . \quad (19)$$

Let us make explicit the invariance equation (19) for the map (10); the other cases can be treated in the same way by suitably choosing the parameters  $\lambda_1, \lambda_2, \mu_1, \mu_2$ .

From the first and second equations in (10) we obtain:

$$x_{n+1} - x_n = y_{n+1} , \quad x_n - x_{n-1} = y_n ,$$

which gives

$$x_{n+1} - x_n - \lambda_1(x_n - x_{n-1}) = y_{n+1} - \lambda_1 y_n ,$$

namely

$$x_{n+1} - (1 + \lambda_1)x_n - \lambda_1 x_{n-1} = \mu_1 + \varepsilon V_1(x_n, z_n; \gamma) . \quad (20)$$

A similar computation for the third and fourth equation in (10) gives

$$z_{n+1} - (1 + \lambda_2)z_n - \lambda_2 z_{n-1} = \mu_2 + \varepsilon V_2(x_n, z_n; \gamma) . \quad (21)$$

Since we can limit to consider the equations (20) and (21) in the coordinates  $x_n$  and  $z_n$ , setting  $\underline{\psi} = (\theta, \varphi)$ , we proceed to parametrize an invariant torus with frequency  $\underline{\omega} = (\omega_1, \omega_2) \in \mathbb{R}^2$  by specifying the components of the embedding  $\underline{K}$  in Definition 7 for the coordinates  $x_n$  and  $z_n$  as

$$\begin{aligned} x_n &= \theta_n + u(\theta_n, \varphi_n) \\ z_n &= \varphi_n + v(\theta_n, \varphi_n) \end{aligned} \quad (22)$$

with the property that

$$\theta_{n+1} = \theta_n + 2\pi\omega_1 , \quad \varphi_{n+1} = \varphi_n + 2\pi\omega_2 .$$

From  $y_n = x_n - x_{n-1}$  and  $w_n = z_n - z_{n-1}$ , we obtain that the variables  $y_n, w_n$  can be computed, once  $u, v$  are known:

$$\begin{aligned} y_n &= \omega_1 + u(\theta_n + 2\pi\omega_1, \varphi_n + 2\pi\omega_2) - u(\theta_n, \varphi_n) \\ w_n &= \omega_2 + v(\theta_n + 2\pi\omega_1, \varphi_n + 2\pi\omega_2) - v(\theta_n, \varphi_n) . \end{aligned}$$

Due to (20) and (21), we obtain that the functions  $u$  and  $v$  satisfy the following equations:

$$\begin{aligned}
& u(\theta_n + 2\pi\omega_1, \varphi_n + 2\pi\omega_2) - (1 + \lambda_1)u(\theta_n, \varphi_n) + \lambda_1 u(\theta_n - 2\pi\omega_1, \varphi_n - 2\pi\omega_2) \\
& + (1 - \lambda_1)\omega_1 - \mu_1 - \varepsilon V_1(\theta_n + u(\theta_n, \varphi_n), \varphi_n + v(\theta_n, \varphi_n); \gamma) = 0 \\
& v(\theta_n + 2\pi\omega_1, \varphi_n + 2\pi\omega_2) - (1 + \lambda_2)v(\theta_n, \varphi_n) + \lambda_2 v(\theta_n - 2\pi\omega_1, \varphi_n - 2\pi\omega_2) \\
& + 2\pi(1 - \lambda_2)\omega_2 - \mu_2 - \varepsilon V_2(\theta_n + u(\theta_n, \varphi_n), \varphi_n + v(\theta_n, \varphi_n); \gamma) = 0 .
\end{aligned} \tag{23}$$

The solution of equation (23) in the form of series expansions will be the core topic in Section 6 below.

## 6. LINDSTEDT SERIES AND ANALYTICITY DOMAINS FOR THE INVARIANT TORI

In this Section, we provide the formulae for the computation of the Lindstedt series expansions of the hull functions  $u$ ,  $v$  introduced in (23) as well as of the drift terms.

**6.1. Iterative computation of the Lindstedt series.** We start by expanding the functions  $u$  and  $v$ , as well as the drifts  $\mu_1$  and  $\mu_2$ , in power series of  $\varepsilon$  as

$$\begin{aligned}
u(\theta, \varphi) &= \sum_{j=1}^{\infty} u_j(\theta, \varphi) \varepsilon^j , & \mu_1 &= \sum_{j=0}^{\infty} \mu_{1,j} \varepsilon^j \\
v(\theta, \varphi) &= \sum_{j=1}^{\infty} v_j(\theta, \varphi) \varepsilon^j , & \mu_2 &= \sum_{j=0}^{\infty} \mu_{2,j} \varepsilon^j .
\end{aligned} \tag{24}$$

Inserting (24) in (23) and equating same powers of  $\varepsilon$  up to a given order  $N \in \mathbb{Z}_+$ , we obtain the truncated Lindstedt series:

$$\begin{aligned}
u^{(N)}(\theta, \varphi) &= \sum_{j=1}^N u_j(\theta, \varphi) \varepsilon^j , & \mu_1^{(N)} &= \sum_{j=0}^N \mu_{1,j} \varepsilon^j \\
v^{(N)}(\theta, \varphi) &= \sum_{j=1}^N v_j(\theta, \varphi) \varepsilon^j , & \mu_2^{(N)} &= \sum_{j=0}^N \mu_{2,j} \varepsilon^j .
\end{aligned} \tag{25}$$

Let us introduce the operators  $E_{1,\mu_1}(u, v)$ ,  $E_{2,\mu_2}(u, v)$  as the left hand sides of (23). Then, we can say that  $u^{(N)}$ ,  $v^{(N)}$  in (25) are such that

$$\|E_{1,\mu_1}(u^{(N)}, v^{(N)})\| = O(|\varepsilon|^{N+1}) , \quad \|E_{2,\mu_2}(u^{(N)}, v^{(N)})\| = O(|\varepsilon|^{N+1}) .$$

The terms  $u_j$ ,  $v_j$ ,  $\mu_{1,j}$ ,  $\mu_{2,j}$  in (25) can be obtained as follows. Consider the formal expansions of the functions  $V_1$ ,  $V_2$  as

$$\begin{aligned} V_1(\theta + u(\theta, \varphi), \varphi + v(\theta, \varphi); \gamma) &= \sum_{j=0}^{\infty} V_{1,j}(\theta, \varphi; \gamma) \varepsilon^j \\ V_2(\theta + u(\theta, \varphi), \varphi + v(\theta, \varphi); \gamma) &= \sum_{j=0}^{\infty} V_{2,j}(\theta, \varphi; \gamma) \varepsilon^j ; \end{aligned} \quad (26)$$

we will give in Section 6.2 an iterative definition of the coefficients  $V_{1,j}$ ,  $V_{2,j}$ . Inserting (24) and (26) into (23), one obtains:

$$\begin{aligned} &\sum_{j=0}^{\infty} u_j(\theta + 2\pi\omega_1, \varphi + 2\pi\omega_2) \varepsilon^j - (1 + \lambda_1) \sum_{j=0}^{\infty} u_j(\theta, \varphi) \varepsilon^j + \lambda_1 \sum_{j=0}^{\infty} u_j(\theta - 2\pi\omega_1, \varphi - 2\pi\omega_2) \varepsilon^j \\ &+ 2\pi(1 - \lambda_1)\omega_1 - \sum_{j=0}^{\infty} \mu_{1,j} \varepsilon^j - \varepsilon \sum_{j=0}^{\infty} V_{1,j}(\theta, \varphi; \gamma) \varepsilon^j = 0 \\ &\sum_{j=0}^{\infty} v_j(\theta + 2\pi\omega_1, \varphi + 2\pi\omega_2) \varepsilon^j - (1 + \lambda_2) \sum_{j=0}^{\infty} v_j(\theta, \varphi) \varepsilon^j + \lambda_2 \sum_{j=0}^{\infty} v_j(\theta - 2\pi\omega_1, \varphi - 2\pi\omega_2) \varepsilon^j \\ &+ 2\pi(1 - \lambda_2)\omega_2 - \sum_{j=0}^{\infty} \mu_{2,j} \varepsilon^j - \varepsilon \sum_{j=0}^{\infty} V_{2,j}(\theta, \varphi; \gamma) \varepsilon^j = 0 . \end{aligned} \quad (27)$$

From the previous relations, equating same powers of  $\varepsilon$ , the following equations are obtained for  $j = 0$ :

$$\begin{aligned} &u_0(\theta + 2\pi\omega_1, \varphi + 2\pi\omega_2) - (1 + \lambda_1)u_0(\theta, \varphi) + \lambda_1 u_0(\theta - 2\pi\omega_1, \varphi - 2\pi\omega_2) \\ &+ 2\pi(1 - \lambda_1)\omega_1 - \mu_{1,0} = 0 \\ &v_0(\theta + 2\pi\omega_1, \varphi + 2\pi\omega_2) - (1 + \lambda_2)v_0(\theta, \varphi) + \lambda_2 v_0(\theta - 2\pi\omega_1, \varphi - 2\pi\omega_2) \\ &+ 2\pi(1 - \lambda_2)\omega_2 - \mu_{2,0} = 0 , \end{aligned} \quad (28)$$

while for  $j > 0$  the equations become:

$$\begin{aligned} &u_j(\theta + 2\pi\omega_1, \varphi + 2\pi\omega_2) - (1 + \lambda_1)u_j(\theta, \varphi) + \lambda_1 u_j(\theta - 2\pi\omega_1, \varphi - 2\pi\omega_2) \\ &- \mu_{1,j} = V_{1,j-1}(\theta, \varphi; \gamma) \\ &v_j(\theta + 2\pi\omega_1, \varphi + 2\pi\omega_2) - (1 + \lambda_2)v_j(\theta, \varphi) + \lambda_2 v_j(\theta - 2\pi\omega_1, \varphi - 2\pi\omega_2) \\ &- \mu_{2,j} = V_{2,j-1}(\theta, \varphi; \gamma) . \end{aligned} \quad (29)$$



**Remark 8.** Notice that, the coefficients  $V_{i,k-1}$  at the right hand side of (29) depend only on the previously computed coefficients  $u_0, u_1, \dots, u_{k-1}, v_0, v_1, \dots, v_{k-1}$ .

At the order  $j = 0$ , a solution of (28) is given by

$$\mu_{1,0} = 2\pi(1 - \lambda_1)\omega_1, \quad \mu_{2,0} = 2\pi(1 - \lambda_2)\omega_2,$$

while we can take  $u_0 := 0$ , and  $v_0 := 0$ .

For  $k \geq 1$ , recalling that  $\underline{\psi} := (\theta, \varphi)$  and  $\underline{\omega} := (\omega_1, \omega_2)$ , the cohomology equations (29) are of the following form

$$g(\underline{\psi} + 2\pi\underline{\omega}) - (1 + \lambda)g(\underline{\psi}) + \lambda g(\underline{\psi} - 2\pi\underline{\omega}) - \mu = \eta(\underline{\psi}; \gamma), \quad (30)$$

where the unknowns are the function  $g : \mathbb{T}^2 \rightarrow \mathbb{C}$  and the scalar  $\mu \in \mathbb{C}$ , whereas the function  $\eta : \mathbb{T}^2 \rightarrow \mathbb{R}$  and the parameters  $\gamma, \lambda \in \mathbb{R}$  are given. Introducing the notation

$$\mathcal{L}_{\lambda, \underline{\omega}} g(\underline{\psi}) := g(\underline{\psi} + 2\pi\underline{\omega}) - (1 + \lambda)g(\underline{\psi}) + \lambda g(\underline{\psi} - 2\pi\underline{\omega}), \quad (31)$$

we have the following Lemma.

**Lemma 9.** Given  $\lambda \in \mathbb{C}$ , such that  $|\lambda| \neq 1$ , let  $\underline{\omega} \in \mathbb{R}^2$  be a Diophantine vector and  $\eta : \mathbb{T}^2 \rightarrow \mathbb{C}$  be an analytic function. Then, the equation

$$\mathcal{L}_{\lambda, \underline{\omega}} g(\underline{\psi}) - \mu = \eta(\underline{\psi}; \gamma) \quad (32)$$

has a unique (zero average) solution given by

$$\begin{aligned} \mu &= -\hat{\eta}_0(\gamma) \\ g(\underline{\psi}) &= \sum_{\underline{k} \in \mathbb{Z}^2 \setminus \{0\}} \frac{\hat{\eta}_{\underline{k}}(\gamma)}{e^{2\pi i \underline{\omega} \cdot \underline{k}} - (1 + \lambda) + \lambda e^{-2\pi i \underline{\omega} \cdot \underline{k}}} e^{i \underline{k} \cdot \underline{\psi}}, \end{aligned} \quad (33)$$

where  $\hat{\eta}_{\underline{k}}(\gamma)$  are the Fourier coefficients of  $\eta$ .

*Proof.* Equation (32) can be solved in Fourier space. Consider the Fourier expansions

$$g(\underline{\psi}) = \sum_{\underline{k} \in \mathbb{Z}^2} \hat{g}_{\underline{k}} e^{i \underline{\psi} \cdot \underline{k}}, \quad \eta(\underline{\psi}; \gamma) = \sum_{\underline{k} \in \mathbb{Z}^2} \hat{\eta}_{\underline{k}}(\gamma) e^{i \underline{\psi} \cdot \underline{k}}; \quad (34)$$

inserting (34) into (32), the equation (32) becomes

$$\sum_{\underline{k} \in \mathbb{Z}^2} (e^{2\pi i \underline{\omega} \cdot \underline{k}} - (1 + \lambda) + \lambda e^{-2\pi i \underline{\omega} \cdot \underline{k}}) \hat{g}_{\underline{k}} e^{i \underline{\psi} \cdot \underline{k}} - \mu = \sum_{\underline{k} \in \mathbb{Z}^2} \hat{\eta}_{\underline{k}}(\gamma) e^{i \underline{\psi} \cdot \underline{k}}. \quad (35)$$

Its solution is given by

$$\begin{aligned} \mu &= -\hat{\eta}_0(\gamma) \\ \hat{g}_{\underline{k}} &= \frac{\hat{\eta}_{\underline{k}}(\gamma)}{e^{2\pi i \underline{\omega} \cdot \underline{k}} - (1 + \lambda) + \lambda e^{-2\pi i \underline{\omega} \cdot \underline{k}}}, \quad \underline{k} \neq 0. \end{aligned} \quad (36)$$

Note that the solution is unique if one requires that  $\hat{g}_0 = 0$ .  $\square$

**6.2. Expansions of the function  $V_1$  and  $V_2$ .** To carry out the procedure described in Section 6.1 to determine the Lindstedt series, one needs to compute the formal expansion in (26) for the functions  $V_1(\theta + u(\theta, \varphi), \varphi + v(\theta, \varphi); \gamma)$  and  $V_2(\theta + u(\theta, \varphi), \varphi + v(\theta, \varphi); \gamma)$ , where, for example, we can take  $V_1$  and  $V_2$  as in (9), that we rewrite as

$$V_1(x, w; \gamma) = \sin(x) + \gamma \sin(x - z), \quad V_2(x, w; \gamma) = \sin(z) - \gamma \sin(x - z).$$

Following [17], the formal expansions can be found as follows.

Using the notation in Lemma 9, we are looking for formal solutions to the cohomology equations (23), that we write as

$$\begin{aligned} \mathcal{L}_{\lambda_1, \omega_1} u(\theta, \varphi) - \mu_1 &= \varepsilon V_1(\theta + u(\theta, \varphi), \varphi + v(\theta, \varphi); \gamma) \\ \mathcal{L}_{\lambda_2, \omega_2} v(\theta, \varphi) - \mu_2 &= \varepsilon V_2(\theta + u(\theta, \varphi), \varphi + v(\theta, \varphi); \gamma), \end{aligned} \quad (37)$$

where we used the definition (31). To find expansions of the functions  $V_\ell$  on the right hand side of (37), we consider the Fourier expansions

$$V_\ell(\theta, \varphi) = \sum_{\underline{k} \in \mathbb{Z}^2} \hat{V}_{\ell, \underline{k}} e^{i \underline{k} \cdot (\theta, \varphi)};$$

therefore, we obtain

$$V_\ell(\theta + u(\theta, \varphi), \varphi + v(\theta, \varphi)) = \sum_{\underline{k} \in \mathbb{Z}^2} \hat{V}_{\ell, \underline{k}} e^{i \underline{k} \cdot (\theta + u(\theta, \varphi), \varphi + v(\theta, \varphi))}. \quad (38)$$

Then, we want to find the expansions of the exponentials as

$$e^{i \underline{k} \cdot (\theta + u(\theta, \varphi), \varphi + v(\theta, \varphi))} = \sum_{j=0}^{\infty} b_j^{\underline{k}}(\theta, \varphi) \varepsilon^j \quad (39)$$

for suitable coefficients  $b_j^{\underline{k}}$  which are determined as follows.

Taking the derivative on both sides of (39), we obtain

$$i \underline{k} \cdot \left( \frac{d}{d\varepsilon} u(\theta, \varphi), \frac{d}{d\varepsilon} v(\theta, \varphi) \right) e^{i \underline{k} \cdot (\theta + u(\theta, \varphi), \varphi + v(\theta, \varphi))} = \sum_{j=0}^{\infty} (j+1) b_{j+1}^{\underline{k}}(\theta, \varphi) \varepsilon^j. \quad (40)$$

Using the formal expansions of  $u$ ,  $v$ , together with (39), we have

$$\begin{aligned} i \underline{k} \cdot \left( \sum_{j=0}^{\infty} (j+1) u_{j+1} \varepsilon^j, \sum_{j=0}^{\infty} (j+1) v_{j+1} \varepsilon^j \right) \sum_{j=0}^{\infty} b_j^{\underline{k}} \varepsilon^j &= \sum_{j=0}^{\infty} (j+1) b_{j+1}^{\underline{k}} \varepsilon^j \\ \sum_{j=0}^{\infty} i \underline{k} \cdot \left( \sum_{h=0}^j (h+1) u_{h+1} b_{j-h}^{\underline{k}}, \sum_{h=0}^j (h+1) v_{h+1} b_{j-h}^{\underline{k}} \right) \varepsilon^j &= \sum_{j=0}^{\infty} (j+1) b_{j+1}^{\underline{k}} \varepsilon^j. \end{aligned} \quad (41)$$

Thus, the following relations follow for  $j \geq 0$ :

$$\begin{aligned} b_0^k(\theta, \varphi) &= e^{i\mathbf{k} \cdot (\theta, \varphi)} \\ b_{j+1}^k &= \frac{i}{j+1} \mathbf{k} \cdot \left( \sum_{h=0}^j (h+1) u_{h+1} b_{j-h}^k, \sum_{h=0}^j (h+1) v_{h+1} b_{j-h}^k \right). \end{aligned} \quad (42)$$

Such expressions, together with (39), yield the expansions (38) for the functions  $V_1$  and  $V_2$ .

**6.3. Explicit cohomology equations.** Using (38) and (39), we obtain that equations (37) can be written as

$$\begin{aligned} \mathcal{L}_{\lambda_1, \underline{\omega}_1} u(\theta, \varphi) - \mu_1 &= \varepsilon \sum_{\mathbf{k} \in \mathbb{Z}^2} \hat{V}_{1, \mathbf{k}} e^{i\mathbf{k} \cdot (\theta + u, \varphi + v)} = \sum_{\mathbf{k} \in \mathbb{Z}^2} \hat{V}_{1, \mathbf{k}} \sum_{j=0}^{\infty} b_j^k(\theta, \varphi) \varepsilon^{j+1} \\ \mathcal{L}_{\lambda_2, \underline{\omega}_2} v(\theta, \varphi) - \mu_2 &= \varepsilon \sum_{\mathbf{k} \in \mathbb{Z}^2} \hat{V}_{2, \mathbf{k}} e^{i\mathbf{k} \cdot (\theta + u, \varphi + v)} = \sum_{\mathbf{k} \in \mathbb{Z}^2} \hat{V}_{2, \mathbf{k}} \sum_{j=0}^{\infty} b_j^k(\theta, \varphi) \varepsilon^{j+1}. \end{aligned} \quad (43)$$

Writing  $u, v, \mu_1, \mu_2$  as formal series in  $\varepsilon$  and matching the coefficients of the same order in (43), one is led to solve the following cohomology equations

$$\begin{aligned} \mathcal{L}_{\lambda_1, \underline{\omega}_1} u_j(\theta, \varphi) - \mu_{1,j} &= \sum_{\mathbf{k} \in \mathbb{Z}^2} \hat{V}_{1, \mathbf{k}} b_{j-1}^k(\theta, \varphi) \\ \mathcal{L}_{\lambda_2, \underline{\omega}_2} v_j(\theta, \varphi) - \mu_{2,j} &= \sum_{\mathbf{k} \in \mathbb{Z}^2} \hat{V}_{2, \mathbf{k}} b_{j-1}^k(\theta, \varphi), \end{aligned} \quad (44)$$

whose solution is obtained using Lemma 9. Once  $u_j, v_j$  are computed from (44), one obtains the formal solutions  $u, v, \mu_1, \mu_2$  of (23), as in (24).

**6.4. Analyticity domains and breakdown of attractors.** In this Section, we provide some results for the standard maps introduced in Section 3. Precisely, for a fixed frequency vector, say  $\underline{\omega}$ , we proceed along the following steps:

- A) we compute the Lindstedt series expansion up to a given order  $N$  according to the procedure described at the beginning of Section 6;
- B) we analyze the behavior of the coefficients of the Lindstedt series to provide an estimate of the radius of convergence;
- C) we determine the Padé approximants (see Appendix A) associated to the Lindstedt series to order  $N$  and we draw the poles in the complex plane  $(\varepsilon_r, \varepsilon_i)$ .

Concerning step  $B$ ), we notice that the radius of convergence  $\rho$  of the Lindstedt series in the complex  $\varepsilon$ -plane can be approximated as

$$\rho(\omega) = \inf_{\theta \in \mathbb{T}} (\limsup_{n \rightarrow \infty} |u_n(\theta)|^{\frac{1}{n}})^{-1}.$$

In practical computations, we will compute an approximation to the radius of convergence only for a specific value of  $\theta$ , say  $\bar{\theta} = 1$ :

$$\rho(\omega; \bar{\theta}) = (\limsup_{n \rightarrow \infty} |u_n(\bar{\theta})|^{\frac{1}{n}})^{-1}.$$

**6.5. Radius of convergence and Padé approximants for the 2-dim case.** The Lindstedt series in step  $A$ ) are determined at orders  $N = 128, 256, 512$  and using 30 or 60 digits of precision.

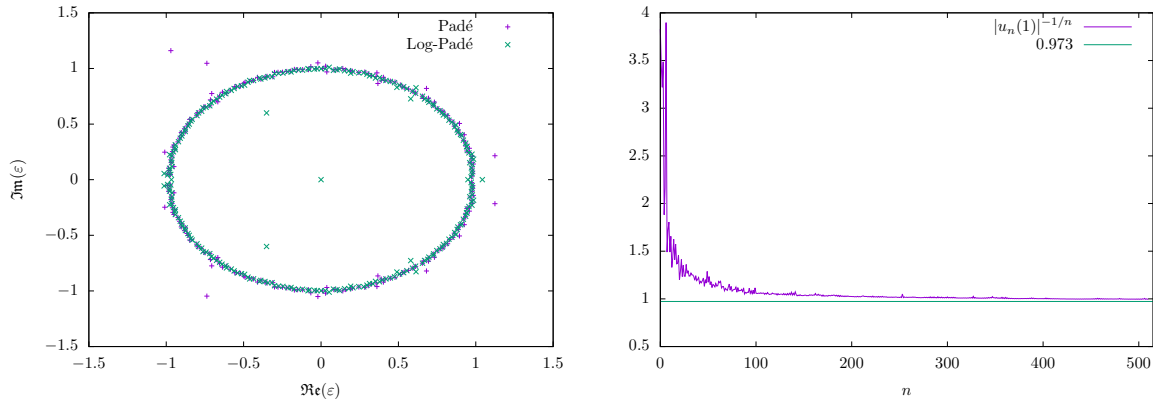


FIGURE 1. Map (7) with  $V(x) = \sin(x)$ ,  $\omega = \frac{\sqrt{5}-1}{2}$ ,  $\lambda = 0.8$ . Left panel: Padé approximants with  $N = 512$ . Right panel: convergence of the Lindstedt coefficients.

Figure 1 refers to the map (7) with  $\omega = \frac{\sqrt{5}-1}{2}$ ,  $\lambda = 0.8$ ; the left panel shows the Padé approximants after computing the Lindstedt series up to the order  $N = 512$  and the right panel shows the values  $|u_n(\bar{\theta})|^{-\frac{1}{n}}$  with  $\bar{\theta} = 1$  and  $n = 1, \dots, 512$ . The breakdown threshold found in [10] for this sample case was  $\varepsilon = 0.973$ , which is consistent with the radius of convergence in the right panel of Figure 1 and with the threshold determined in the left panel of Figure 1 as the intersection of the analyticity domain with the positive abscissa ([5], [21]).

It is known that Padé approximants are better suited to approximate functions with poles, rather than functions with branch points ([4]). The theoretical and numerical evidence presented in [20], [21] indicates that the boundaries of the domains of analyticity of invariant circles could be described as an accumulation of branch points. As a

consequence, a logarithmic Padé approximation is better suited to compute singularities that are branch points; we follow [21] for the computation of the logarithmic Padé approximation. If a function  $f(z)$  has a branch point singularity at  $z = 1/\alpha$ , then

$$f(z) = A(1 - \alpha z)^\gamma + g(z) ,$$

where  $g(z)$  is an analytic function at  $z = 1/\alpha$  and  $\gamma < 0$ . Consider the function

$$F(z) := \frac{d}{dz} \ln(f(z)) = \frac{f'(z)}{f(z)} ;$$

then, one has that for  $z$  close to  $1/\alpha$ :

$$F(z) = \frac{f'(z)}{f(z)} \approx \frac{\gamma}{z - (1/\alpha)} .$$

That is, one expects that a Padé approximant for  $F(z)$  exhibits a pole at  $z = 1/\alpha$  with residue  $\gamma$ . Finally, to get an  $[M, N]$  Padé approximant of  $F(z)$  one needs to find polynomials  $P^{(M)}(z)$  and  $Q^{(N)}(z)$  of degrees  $M$  and  $N$ , respectively, satisfying

$$\frac{f'(z)}{f(z)} = \frac{P^{(M)}(z)}{Q^{(N)}(z)} + O(z^{M+N+1})$$

and  $Q^{(N)}(0) = 1$ .

**Remark 10.** *The order of the branch point,  $\gamma$ , could be estimated by using Padé approximants on different functions related to  $F(z)$ . For example, close to  $z = 1/\alpha$ ,*

$$\left(z - \frac{1}{\alpha}\right) \frac{f'(z)}{f(z)} \approx \gamma .$$

Figure 2, upper plots, refers to the frequency  $\omega = s^{-1}$ ; the left panel shows the Padé and log-Padé approximants for the one-harmonic case  $V(x) = \sin x$  and for two values of  $\lambda$ ; the radii of convergence of the Lindstedt series agree with the circles shown in Figure 2, upper plots, and they are estimated as  $\varepsilon_c = 0.73$  for  $\lambda = 0.9$  and  $\varepsilon_c = 0.758$  for  $\lambda = 0.8$ , well below the threshold of the golden ratio of Figure 1. Besides, for  $\omega = s^{-1}$  the results for the domain take a sort of flower shape. The results for the two-harmonic case with  $V(x) = \sin x + \frac{1}{3} \sin(3x)$  are shown in the lower panels of Figure 2 for  $\lambda = 0.8$  with  $\omega = \frac{\sqrt{5}-1}{2}$  (left) and  $\omega = s^{-1}$  (right). In the latter case the estimate of the threshold is more difficult, due to the irregular shape of the domain of analyticity.

To analyze the dependence of the domains of analyticity on the choice of the dissipation parameter  $\lambda$ , Figure 3 shows the results of the Padé approximants for the two harmonic potential  $V_{2h}$  and for different values of  $\lambda$ , taking  $\omega = \frac{\sqrt{5}-1}{2}$  (left panel) and  $\omega = s^{-1}$  (right panel). We fixed  $N = 256$  and used 40 digits of precision.

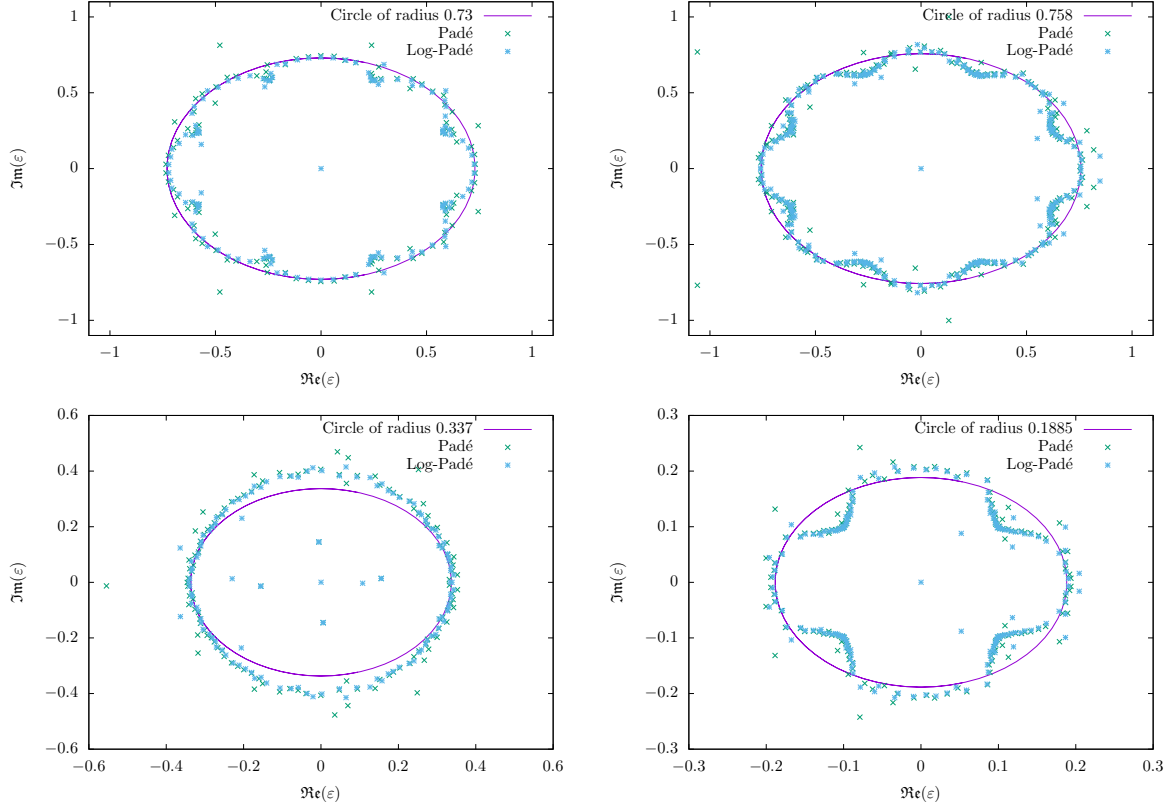


FIGURE 2. Upper plots: map (7) with  $V(x) = \sin(x)$ ,  $\omega = s^{-1}$ . Left:  $\lambda = 0.9$ , poles of Padé and log-Padé approximants with  $N = 256$ , showing also the circle of radius 0.73. Right:  $\lambda = 0.8$ , poles of Padé and log-Padé approximants with  $N = 256$ , showing also the circle of radius 0.758. Lower plots: map (7) with  $V_{2h}(x) = \sin(x) + \frac{1}{3}\sin(3x)$ ,  $\lambda = 0.8$ . Left: poles of Padé and log-Padé approximants with  $N = 256$  and 40 digits of precision for  $\omega = \frac{\sqrt{5}-1}{2}$  and the circle of radius 0.337. Right: poles of Padé and log-Padé approximants with  $N = 341$  and 70 digits of precision for  $\omega = s^{-1}$  and the circle of radius 0.1885.

**6.6. Padé approximants for the 4-dim case.** For the 4-dim maps, the computations are definitely more demanding; for this reason, the Lindstedt series in step A) are determined only up to order  $N = 128$ , and  $N = 256$  in some cases with at least 60 digits of precision.

We first consider the maps (8), (10), (11) with different values of the parameters and with the potentials containing one harmonic and the coupling:  $V_1(\theta, \varphi) = \sin(\theta) + \gamma \sin(\theta - \varphi)$ ,  $V_2(\theta, \varphi) = \sin(\varphi) - \gamma \sin(\theta - \varphi)$ . The left panel of Figure 4 refers to the symplectic case with  $\omega_1 = \frac{\sqrt{5}-1}{2}$ ,  $\omega_2 = s^{-1}$ ,  $\gamma = 0.01$ ; it shows the Padé and log-Padé approximants with  $N = 128$ , obtained using 60 digits of precision. The radius of the

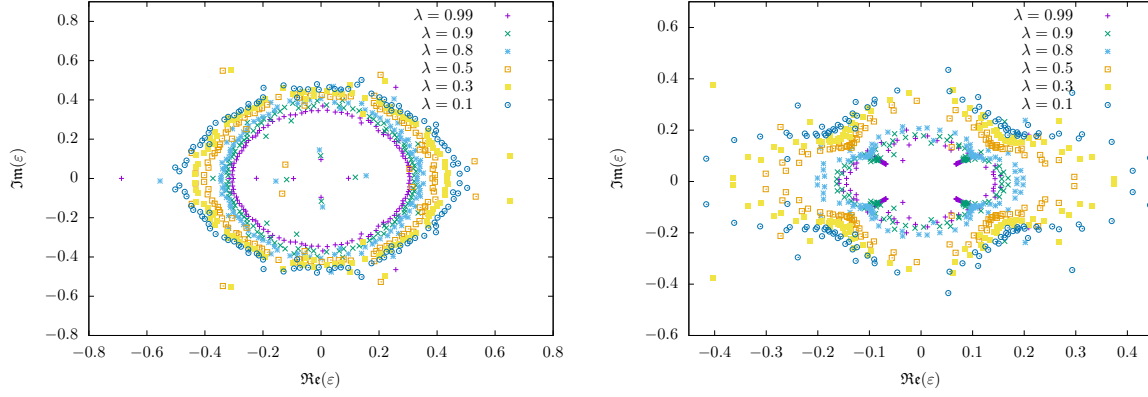


FIGURE 3. Map (7) with  $V_{2h}(x) = \sin x + \frac{1}{3} \sin(3x)$  for different values of  $\lambda$  with  $N = 256$  and 40 digits of precision. The plots display the poles of the Padé approximants for  $N = 256$ . Left panel:  $\omega = \frac{\sqrt{5}-1}{2}$ . Right panel:  $\omega = s^{-1}$ .

domain, confirmed by the convergence of the Lindstedt coefficients (not shown here), is about  $\varepsilon_c = 0.53$ . The right panel of Figure 4 refers to the mixed map (11) with the same frequency vector, but with  $\lambda_1 = 1$  and  $\lambda_2 = 0.8$ . In this case, the radius of convergence is about  $\varepsilon_c = 0.68$ .

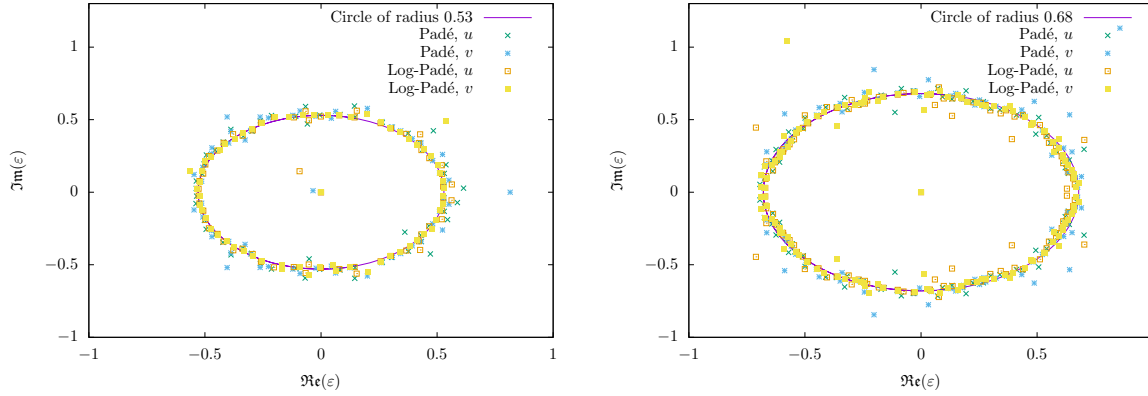


FIGURE 4. Map (8) (left) and (11) (right) with  $\omega_1 = \frac{\sqrt{5}-1}{2}$ ,  $\omega_2 = s^{-1}$ ,  $\gamma = 0.01$ . The plots display the poles of the Padé and log-Padé approximants for  $N = 256$ . In the right panel we set  $\lambda_1 = 1$ ,  $\lambda_2 = 0.8$ .

Finally, we show in Figure 5 the results for the dissipative case with  $\lambda_1 = 0.8$  and  $\lambda_2 = 0.7$ . For the frequency vector with  $\omega_1 = \frac{\sqrt{5}-1}{2}$ ,  $\omega_2 = s^{-1}$  (left panel), the poles of Padé and log-Padé approximants are spread within a ring with radii approximately equal to 0.67 and 0.76. The domain becomes much less regular even by just changing the second component of the frequency vector as  $\omega_2 = s - 1$  (right panel); in this case the ring has radii 0.67 and 0.88.

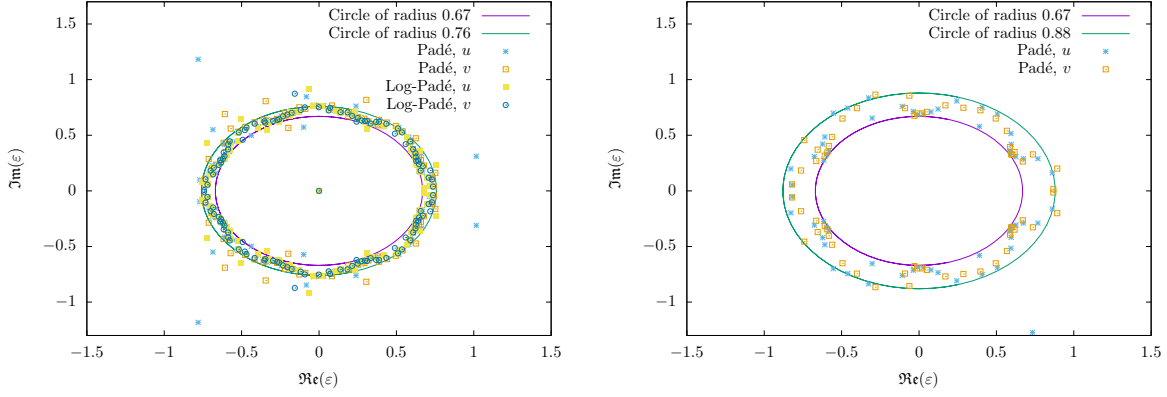


FIGURE 5. Left: Map (10) with  $\omega_1 = \frac{\sqrt{5}-1}{2}$ ,  $\omega_2 = s^{-1}$ ,  $\lambda_1 = 0.8$ ,  $\lambda_2 = 0.7$ ,  $\gamma = 0.01$ . Poles of the Padé and log-Padé approximants for  $N = 256$ . Right: Map (10) with  $\omega_1 = \frac{\sqrt{5}-1}{2}$ ,  $\omega_2 = s - 1$ ,  $\lambda_1 = 0.8$ ,  $\lambda_2 = 0.7$ , and  $\gamma = 0.0005$ . Poles of Padé approximants for  $N = 128$ ,

	$(\varpi, s^{-1})$	$(\varpi, s - 1)$	$\underline{\omega}_a$	$\underline{\omega}_c$	$\underline{\omega}_u$
symplectic	0.53	0.37	0.46	0.38	0.48
mixed	0.68	0.48 – 0.55	0.46	0.50	0.47
dissipative	0.67 – 0.76	0.68	0.63	0.66	0.67

TABLE 2. Breakdown thresholds for different frequency vectors, estimated by computing the radius of convergence of the Lindstedt coefficients with  $N = 128$ . Dissipative:  $\lambda_1 = 0.8$ ,  $\lambda_2 = 0.7$ ,  $\gamma = 0.01$ . Mixed:  $\lambda_1 = 1$ ,  $\lambda_2 = 0.8$ ,  $\gamma = 0.01$ . Symplectic:  $\lambda_1 = 1$ ,  $\lambda_2 = 1$ ,  $\gamma = 0.01$

We studied also other frequency vectors by computing the Lindstedt series, the analyticity domains through the Padé and log-Padé approximants, and providing an estimate of the break-down threshold by looking at the radius of convergence of the Lindstedt coefficients with  $N = 128$ . The results of such thresholds are summarized in Table 2, which shows that the radii tend to increase, as the 4-dim map switches from symplectic to mixed to dissipative, when at least one component of the frequency vector is a good irrational number.

Furthermore, we provide in Table 3 some results concerning the dependence of the thresholds on the coupling parameter. Precisely, we consider the frequency  $(\varpi, s - 1)$  and we vary the coupling parameter  $\gamma$  on a set of values.

We conclude by mentioning some results for potentials with two harmonic and a coupling, say  $V_1(\theta, \varphi) = \sin(\theta) + \frac{1}{3} \sin(3\theta) + \gamma \sin(\theta - \varphi)$ ,  $V_2(\theta, \varphi) = \sin(\varphi) + \frac{1}{3} \sin(3\varphi) -$



$\gamma$	dissipative	mixed	symplectic
0.0001	0.68 – 0.81	0.63 – 0.81	0.63
0.0005	0.67 – 0.88	0.63 – 0.76	0.58
0.001	0.68 – 0.79	0.72	0.53
0.005	0.66 – 0.74	0.54 – 0.60	0.42
0.01	0.68	0.48 – 0.55	0.37
0.05	0.60	0.34 – 0.41	0.28
0.1	0.53	0.24 – 0.38	0.25
0.25	0.39 – 0.43	0.15 – 0.44	0.21
0.5	0.30 – 0.33	0.1 – 0.28	0.19

TABLE 3. Breakdown thresholds for the frequency  $(\varpi, s - 1)$  and for different values of the coupling parameter  $\gamma$ . Dissipative:  $\lambda_1 = 0.8$ ,  $\lambda_2 = 0.7$ . Mixed:  $\lambda_1 = 1$ ,  $\lambda_2 = 0.8$ . Symplectic:  $\lambda_1 = 1$ ,  $\lambda_2 = 1$ .

$\gamma \sin(\theta - \varphi)$ . The plots of Figure 6 show the results for the symplectic case, map (8), with frequency  $\omega_1 = \frac{\sqrt{5}-1}{2}$ ,  $\omega_2 = s^{-1}$  and with  $\gamma = 0.01$ . The poles of the Padé approximants (upper left) are computed up to the order  $N = 85$  with a precision of at least 50 digits; the radii of convergence of the Lindstedt series coefficients (upper right) are computed up to  $N = 85$ . The radius of convergence can be estimated as about equal to 0.105; for the mixed case (lower left), we obtain a ring between 0.14 and 0.17, while for the dissipative case (lower right) the domain becomes very irregular.

## 7. NEWTON'S METHOD AND SOBOLEV'S CRITERION

This Section is devoted to the presentation of Newton's method for the 2-dim and 4-dim cases; we also describe the Sobolev's criterion to find the breakdown threshold and we provide some results for the 2-dim and 4-dim maps.

**7.1. Newton's method for the 2-dim map.** For the dissipative 2-dim standard map (7), we have borrowed a Newton's method that have been implemented very successfully in [10]. It consists in finding a hull function  $u : \mathbb{T} \longrightarrow \mathbb{R}^2$  and a drift parameter  $\mu \in \mathbb{R}$  satisfying the equation

$$u(\theta + 2\pi\omega) - (1 + \lambda)u(\theta) + \lambda u(\theta - 2\pi\omega) = \mu + \varepsilon V(\theta + u(\theta)). \quad (45)$$

The details about the construction and implementation of the Newton's method can be found in [10].

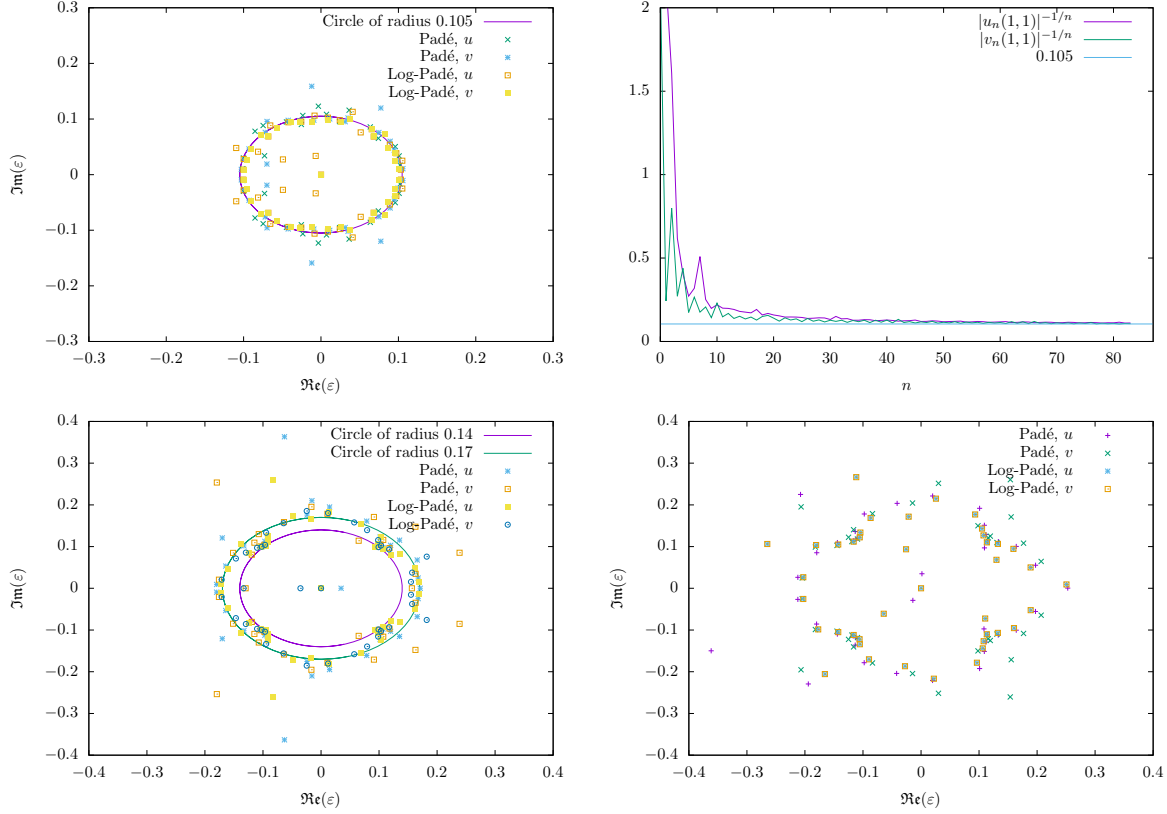


FIGURE 6. Upper plots: map (8) with  $\omega_1 = \frac{\sqrt{5}-1}{2}$ ,  $\omega_2 = s^{-1}$ ,  $\gamma = 0.01$ ,  $N = 85$ ,  $\bar{\theta} = (1, 1)$ . Left panel: Poles of the Padé approximants for  $N = 85$ . Right panel: radius of convergence of the Lindstedt coefficients with  $N = 85$  and  $\bar{\theta} = (1, 1)$ . Lower plots: Padé and log-Padé approximants for  $N = 85$ ,  $\omega_1 = \frac{\sqrt{5}-1}{2}$ ,  $\omega_2 = s^{-1}$ ,  $\gamma = 0.01$  and  $\lambda_1 = 1$ ,  $\lambda_2 = 0.8$  (left),  $\lambda_1 = 0.8$ ,  $\lambda_2 = 0.7$  (right).

**7.2. Newton's method for 4-dim map.** In the 4-dim case, we present a procedure borrowed from [13] to find, through a Newton's method, the parameterization of an invariant torus. In the following lines we give a brief explanation of the construction of the corrections at each step of the Newton's method.

Consider the map  $f_{\mu,\varepsilon} : \mathbb{T}^2 \times \mathbb{R}^2 \longrightarrow \mathbb{T}^2 \times \mathbb{R}^2$  given by

$$f_{\mu,\varepsilon} \begin{pmatrix} x \\ z \\ y \\ w \end{pmatrix} = \begin{pmatrix} x + \lambda y + \mu_1 + \varepsilon V_1(x, z) \\ z + \lambda w + \mu_2 + \varepsilon V_2(x, z) \\ \lambda y + \mu_1 + \varepsilon V_1(x, z) \\ \lambda w + \mu_2 + \varepsilon V_2(x, z) \end{pmatrix}. \quad (46)$$

In this Section, we limit to consider a family of conformally symplectic maps  $f_{\underline{\mu},\varepsilon}$  with conformal factor  $\lambda$  equal for both components  $y$  and  $w$ . We remark that the extension to the case of different conformal factors, say  $\lambda_1, \lambda_2$ , cannot be directly derived from [13].

We look for a parameterization  $\underline{K} : \mathbb{T}^2 \longrightarrow \mathbb{T}^2 \times \mathbb{R}^2$  and a constant vector  $\underline{\mu} \in \mathbb{R}^2$  satisfying the invariance equation

$$\underline{f}_{\underline{\mu}, \varepsilon} \circ \underline{K} = \underline{K} \circ T_{\underline{\omega}}, \quad (47)$$

where  $T_{\underline{\omega}}(\underline{\theta}) = \underline{\theta} + 2\pi\underline{\omega}$ . Note that if such  $\underline{K}$  and  $\underline{\mu}$  satisfying (47) exist, then there exists an invariant torus, parameterized by  $\underline{K}$ , whose dynamics is conjugated to a rotation by  $\underline{\omega}$ .

The Newton's method we consider takes advantage of the so-called "automatic reducibility": in a neighborhood of an invariant torus there exists an explicit change of coordinates that makes the linearization of the invariance equation (47) into an equation with constant coefficients (see equation (56) below). That is, defining  $M(\underline{\theta})$  as the 4x4 matrix

$$M(\underline{\theta}) = [D\underline{K}(\underline{\theta})|J^{-1}D\underline{K}(\underline{\theta})N(\underline{\theta})], \quad (48)$$

where  $N(\underline{\theta}) = [D\underline{K}(\underline{\theta})^\top D\underline{K}(\underline{\theta})]^{-1}$ , then, if  $\underline{K}$  and  $\underline{\mu}$  satisfy (47), one has that

$$D\underline{f}_{\underline{\mu}, \varepsilon} \circ \underline{K}(\underline{\theta})M(\underline{\theta}) = M(\underline{\theta} + 2\pi\underline{\omega}) \begin{pmatrix} Id & S(\underline{\theta}) \\ 0 & \lambda Id \end{pmatrix}, \quad (49)$$

where  $S(\underline{\theta})$  is an explicit function depending on  $D\underline{K}(\underline{\theta})$  and  $D\underline{f}_{\underline{\mu}, \varepsilon} \circ \underline{K}(\underline{\theta})$ .

Next, we briefly describe the quasi-Newton's method used to find solutions of (47); a detailed exposition of such method can be found in [13]. We start with an approximate solution of (47), say

$$\underline{f}_{\underline{\mu}, \varepsilon} \circ \underline{K} - \underline{K} \circ T_{\underline{\omega}} = \underline{E}, \quad (50)$$

where the error in the approximation,  $\underline{E}$ , is supposed to be small. The Newton's method introduced in [13] consists in finding corrections  $\underline{\Delta}$  and  $\underline{\sigma}$  to  $\underline{K}$  and  $\underline{\mu}$ , respectively, such that the approximated solution of (47) associated to  $\underline{K} + \underline{\Delta}$ ,  $\underline{\mu} + \underline{\sigma}$  quadratically reduces the error. Taking into account that

$$\underline{f}_{\underline{\mu} + \underline{\sigma}, \varepsilon} \circ (\underline{K} + \underline{\Delta}) = \underline{f}_{\underline{\mu}, \varepsilon} \circ \underline{K} + [D\underline{f}_{\underline{\mu}, \varepsilon} \circ \underline{K}]\underline{\Delta} + [D_{\underline{\mu}}\underline{f}_{\underline{\mu}, \varepsilon} \circ \underline{K}]\underline{\sigma} + O(\|\underline{\Delta}\|^2) + O(\|\underline{\sigma}\|^2), \quad (51)$$

Newton's method consists in finding  $\underline{\Delta}$  and  $\underline{\sigma}$  satisfying

$$[D\underline{f}_{\underline{\mu}, \varepsilon} \circ \underline{K}]\underline{\Delta} - \underline{\Delta} \circ T_{\underline{\omega}} + [D_{\underline{\mu}}\underline{f}_{\underline{\mu}, \varepsilon} \circ \underline{K}]\underline{\sigma} = -\underline{E}. \quad (52)$$

Instead of solving (52) the main idea in [13] is to use the automatic reducibility to find an approximate solution of (47), that still leads to a quadratically convergent procedure. Using the matrix  $M$  defined in (48), a change of variables in (52) is introduced by setting

$$\underline{\Delta} = M\underline{W} \quad (53)$$

with  $M$  as in (48). In the new unknowns  $\underline{W}$  and  $\underline{\sigma}$ , equation (52) transforms into

$$[D_{\underline{\mu}, \varepsilon} f \circ \underline{K}] M \underline{W} - (M \circ T_{\underline{\omega}})(\underline{W} \circ T_{\underline{\omega}}) + [D_{\underline{\mu}, \varepsilon} f \circ \underline{K}] \underline{\sigma} = -\underline{E}. \quad (54)$$

Then using (49), and ignoring an error term in (49) coming from the fact that  $\underline{K}$ ,  $\underline{\mu}$  is an approximate solution to (47), one obtains

$$M \circ T_{\underline{\omega}} \left[ \begin{pmatrix} Id & S(\theta) \\ 0 & \lambda Id \end{pmatrix} \underline{W} - \underline{W} \circ T_{\underline{\omega}} \right] + [D_{\underline{\mu}, \varepsilon} f \circ \underline{K}] \underline{\sigma} = -\underline{E}. \quad (55)$$

As it is noted in [13], equation (55) reduces to difference equations with constant coefficients, so that it can be solved efficiently by using Fourier methods. Using the notation  $\underline{W} = (W_1, W_2)^\top$ ,  $\underline{\tilde{E}} = (M^{-1} \circ T_{\underline{\omega}}) \underline{E} := (\tilde{E}_1, \tilde{E}_2)^\top$ , and  $\tilde{A} = (M^{-1} \circ T_{\underline{\omega}}) D_{\underline{\mu}, \varepsilon} f \circ \underline{K} := [\tilde{A}_1 | \tilde{A}_2]$ , equation (55) can be expressed in components as

$$\begin{aligned} \underline{W}_1 - \underline{W}_1 \circ T_{\underline{\omega}} &= -S \underline{W}_2 - \tilde{E}_1 - (\tilde{A} \underline{\sigma})_1 \\ \lambda \underline{W}_2 - \underline{W}_2 \circ T_{\underline{\omega}} &= -\tilde{E}_2 - (\tilde{A} \underline{\sigma})_2. \end{aligned} \quad (56)$$

The system of equations (56) has an upper triangular structure and the way to solve it is summarized in Algorithm 13 described in Appendix B.

Implementing Newton's method to find approximations of  $\underline{K}$ ,  $\underline{\mu}$ , and computing suitable norms of such approximations will allow us to get information on the breakdown threshold of invariant attractors (see Section 7.3). The algorithm to implement one step of the Newton's method is thoroughly explained in [13], we have included it in Appendix B for the sake of completeness.

**7.3. Sobolev's criterion for the 4-dim case.** Given a periodic function  $f$  on  $\mathbb{T}^2$ , we consider a sample of points on the regular grid of size  $\underline{L} = (L_1, L_2)$

$$\theta_j := (\theta_{j_1}, \theta_{j_2}) = \left( \frac{2\pi j_1}{L_1}, \frac{2\pi j_2}{L_2} \right),$$

where  $\underline{j} = (j_1, j_2) \in \mathbb{Z}^2$  and  $0 \leq j_1 < L_1$ ,  $0 \leq j_2 < L_2$ . The total number of points is given by  $L_D = L_1 L_2$ . To implement numerically the Newton step described in Section 7.2, we consider Fourier series of the form  $f(\theta) = \sum_{\underline{k}'} \hat{f}_{\underline{k}'} e^{i \underline{k}' \cdot \underline{\theta}}$  with the multi-index  $\underline{k}' = (k'_1, k'_2)$  given as follows:

$$k'_l = \begin{cases} k_l & \text{if } 0 \leq k_l \leq L_l/2 \\ k_l - L_l & \text{if } L_l/2 < k_l < L_l \end{cases}.$$

Note that the truncated Fourier series coincides with the Discrete Fourier Transform on the points of the grid. Following [25], we also introduce the tail in the  $l$ -angle of the

truncated Fourier series as follows:

$$\text{tail}_l(\{\hat{f}_{\underline{k}}\}) := \sum_{\underline{C}_l} |\hat{f}_{\underline{k}}|, \quad l = 1, 2,$$

where  $\underline{C}_l$  is defined as the set of multi-indices

$$\underline{C}_l = \left\{ \underline{k} = (k_1, k_2) : \frac{L_l}{4} \leq k_l \leq \frac{3L_l}{4} \right\}.$$

To control the quality of the approximation we ask this tail to be small.

The rigorous results described in [13] and [12] provide an algorithm to approximate the analyticity breakdown. Given a well-behaved approximate solution to (47), there are true solutions in a neighborhood and, moreover, close to the breakdown the Sobolev semi-norms must blow up. Let the Fourier expansion of a function  $f : \mathbb{T}^2 \rightarrow \mathbb{R}$  be written as  $f(\underline{\psi}) = \sum_{\underline{k} \in \mathbb{Z}^2} \hat{f}_{\underline{k}} e^{i\underline{k} \cdot \underline{\psi}}$  and let  $\|f\|_{L^2} := (\sum_{\underline{k} \in \mathbb{Z}^2} |\hat{f}_{\underline{k}}|^2)^{1/2}$ . Then, following [7] we define the semi-norms

$$\begin{aligned} \|f\|_{r,\parallel} &:= \|(2\pi\underline{\omega} \cdot \nabla)^r f\|_{L^2} \\ \|f\|_{r,\perp} &:= \|(2\pi\underline{\omega}^\perp \cdot \nabla)^r f\|_{L^2}, \end{aligned}$$

where  $\underline{\omega} = (\omega_1, \omega_2)$ . For trigonometric polynomials, say  $f^{(N)}(\underline{\psi}) = \sum_{|\underline{k}| \leq N} \hat{f}_{\underline{k}} e^{i\underline{k} \cdot \underline{\psi}}$ , the semi-norms are computed as follows:

$$\|f^{(N)}\|_{r,\parallel} = \left( \sum_{|\underline{k}| \leq N} (2\pi\underline{\omega} \cdot \underline{k})^{2r} |\hat{f}_{\underline{k}}|^2 \right)^{1/2}, \quad \|f^{(N)}\|_{r,\perp} = \left( \sum_{|\underline{k}| \leq N} (2\pi\underline{\omega}^\perp \cdot \underline{k})^{2r} |\hat{f}_{\underline{k}}|^2 \right)^{1/2}.$$

The domain of existence of invariant tori can be computed using an approximate solution of equation (47) with  $\underline{K}_0 = (K_1^0, K_2^0, K_3^0, K_4^0)$  represented by trigonometric polynomials, a regular behavior of the Sobolev norms, as the parameter  $\varepsilon$  increases, provides evidence of the existence of the quasiperiodic orbit. The algorithm to identify the boundary of the existence domain can be described as follows:

**Algorithm 11.** Use  $\underline{K}_0, \underline{\mu}_0$  for the integrable case ( $\varepsilon = 0$ ).

**Repeat**

*Increase the parameter  $\varepsilon$  along the positive real axis*

*Run the Newton step (Algorithm 13)*

**If** *iteration of the Newton step does not converge*

*decrease the increment in the parameter  $\varepsilon$*

**Else** *(Iteration success)*

*Record the values of the parameters and compute the seminorms of the solution*

**If** for any index  $l$ , any of the tails  $\text{tail}_l(\{\hat{K}_{k,i}\})$  exceeds a given value

*Double the number of Fourier coefficients in the  $l$ -angle*

**Until** one of the Sobolev seminorms of the approximate solution exceed a given value

**Remark 12.** We note that Algorithm 11 is also used for the 2-dim case. The only change is that there is only one tail for the hull function that solves (45). Also, in this case the Sobolev norm is defined as  $\|u\|_r := \|\partial_\theta u\|_{L^2}$ , and for a trigonometric polynomial  $u^{(N)}(\theta) = \sum_{|k| \leq N} \hat{u}_k e^{ik\theta}$  the norm is computed as  $\|u^{(N)}\|_r = \left( \sum_{|k| \leq N} k^{2r} |\hat{u}_k|^2 \right)^{1/2}$ .

**7.4. Results for the 2-dim case.** The results of the implementation of the Newton's method and the Sobolev criterion for the 2-dim case are summarized in Figure 7 (upper plots), which shows the Sobolev norm and the Padé approximants, providing an estimate of 0.758 for the breakdown threshold in the case  $\omega = s^{-1}$ ,  $\lambda = 0.8$ . The threshold amounts to 0.1885 for the two harmonics case (lower plots). Additional details for different values of  $\varepsilon$  on the norm of the hull function and the norm of the error are given in Table 4.

TABLE 4. Values of the Sobolev norms for different values of the continuation using two different potentials. Parameters:  $\omega = s^{-1}$ ,  $\lambda = 0.8$ . We have only included the values of  $\varepsilon$  for which the number of Fourier modes were doubled.  $L$  denotes the number of Fourier modes.

$V(x) = \sin(x)$				$V(x) = \sin(x) + \frac{1}{3} \sin(3x)$			
$\varepsilon$	$\ u\ _2$	$\ E\ _\infty$	$L$	$\varepsilon$	$\ u\ _2$	$\ E\ _\infty$	$L$
0.1	0.040	8.7e-10	64	0.01	0.018	1.2e-12	64
0.3	0.169	8.0e-15	128	0.02	0.063	2.7e-12	128
0.5	0.968	5.91e-12	256	0.05	0.377	1.6e-11	256
0.6	2.082	8.0e-10	512	0.09	1.235	8.1e-11	512
0.62	2.405	2.4e-13	1024	0.13	2.671	7.2e-11	1024
0.68	3.664	1.4e-12	2048	0.16	4.218	1.5e-13	2048
0.72	5.566	1.0e-10	4096	0.18	11.59	1.5e-10	4096
0.75	31.638	1.6e-10	8192	0.183	18.198	2.1e-13	8192
0.751	35.510	9.1e-13	16384	0.186	32.664	5.2e-11	16384
0.754	54.069	4.3e-12	32768	0.188	56.853	9.7e-10	32768
0.756	82.410	5.5e-11	65536	0.1881	58.969	2.5e-10	65536
0.757	117.512	4.3e-10	131072	0.1882	61.253	2.8e-10	131072
				0.1883	113.47	3.2e-10	262144

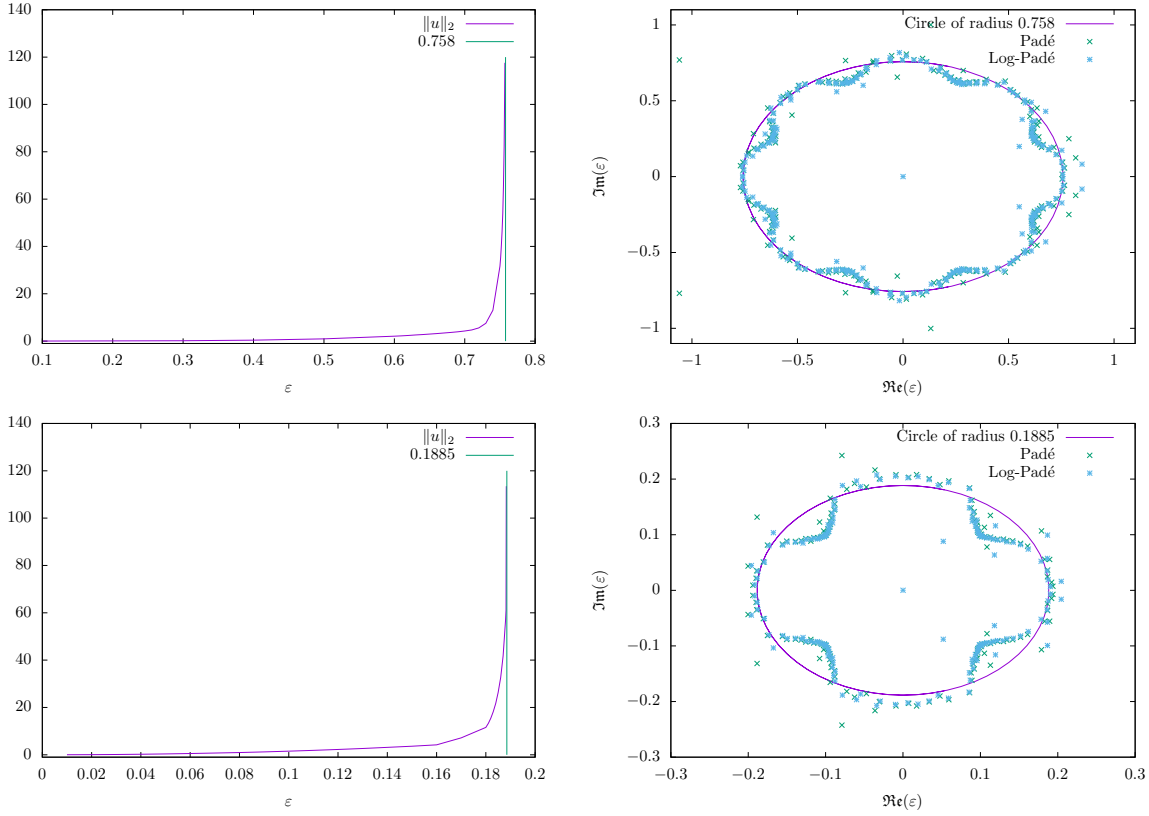


FIGURE 7.  $\omega = s^{-1}$ ,  $\lambda = 0.8$ . Left:  $\|u\|_2$ . Right: poles of the Padé approximants. Upper plots:  $V(x) = \sin(x)$ . Lower plots  $V(x) = \sin(x) + \frac{1}{3}\sin(3x)$ .

**7.5. Results for the 4-dim case.** We consider the conformally symplectic case with  $\lambda_1 = \lambda_2 = 0.8$ . We only monitored the growth of the Sobolev norms for the first two components of the parameterization  $K = (K_1, K_2, K_3, K_4)$ . The results are presented in Table 5 and Figure 8.

## 8. FINDING PERIODIC ORBITS

In this Section, we look for the breakdown threshold of the invariant tori by using the information on the periodic orbits approximating the tori. In fact, the well-known numerical method developed by J. Greene in [24] for the determination of the stochastic transition is based on the conjecture that the tori breakdown when the periodic orbits, with frequency equal to the rational approximants to the frequency of the torus, change from stability to instability. Greene's method was originally developed for the symplectic standard map and later used for other models, including the 2-dim dissipative standard map in [10]. The application of Greene's method to dissipative systems is made difficult

TABLE 5. Map (10) with  $\lambda_1 = \lambda_2 = 0.8$ ,  $\gamma = 0.01$ ,  $\omega_1 = \frac{\sqrt{5}-1}{2}$ ,  $\omega_2 = s^{-1}$ . Values of the Sobolev norms of the first two components of the approximate solution  $K = (K_1, K_2, K_3, K_4)$ . The iteration is successful in Algorithm 11 when the error of the approximation is  $< 10^{-9}$ . The number of Fourier coefficients in the  $l$ -angle is doubled when  $\text{tail}_l < 10^{-13}$ .  $L_l$  denotes the number of Fourier modes used in the angle  $l$ .

$\varepsilon$	$\ K_1\ _{2,\parallel}$	$\ K_2\ _{2,\parallel}$	$\ K_1\ _{2,\perp}$	$\ K_2\ _{2,\perp}$	$L_1$	$L_2$	$\ E\ _\infty$
0.05	0.170	0.453	0.257	0.306	32	32	4.1e-12
0.10	0.343	0.907	0.518	0.614	64	64	6.2e-12
0.15	0.520	1.371	0.786	0.929	64	64	9.9e-12
0.20	0.705	1.890	1.064	1.283	64	64	1.5e-11
0.25	0.901	2.608	1.360	1.770	64	128	2.7e-11
0.30	1.115	3.814	1.681	2.582	128	128	6.1e-11
0.35	1.356	5.897	2.039	3.980	128	128	1.7e-10
0.40	1.634	9.278	2.447	6.247	128	256	5.1e-10
0.45	1.969	14.413	2.926	9.688	128	256	1.0e-16
0.50	2.389	21.866	3.507	14.684	256	256	2.2e-15
0.55	2.959	32.419	4.237	21.755	256	512	5.2e-14
0.60	3.884	48.041	5.202	32.135	256	512	2.7e-11
0.65	6.583	135.349	6.863	83.489	256	1024	9.9e-10
0.675	17.548	491.393	11.618	294.923	512	2048	2.1e-13
0.678	22.731	601.608	14.024	361.202	512	4096	3.3e-11

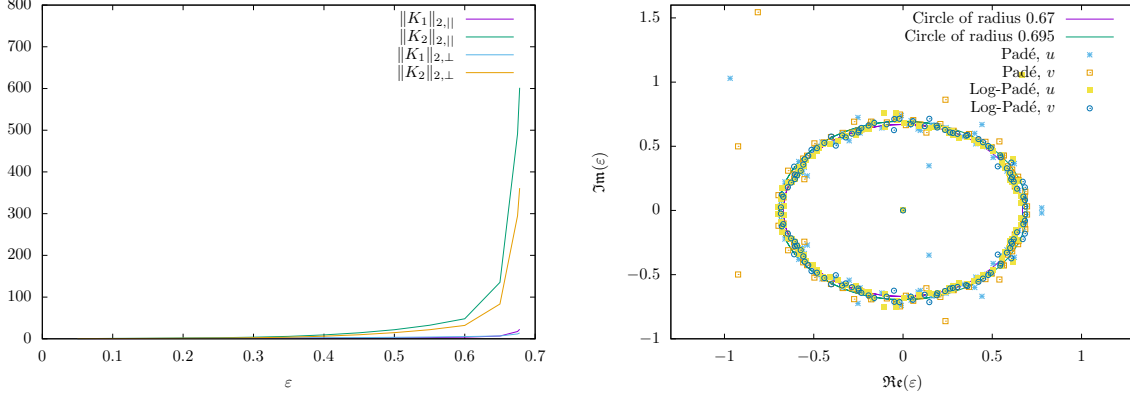


FIGURE 8. Map (10) with  $\omega_1 = \frac{\sqrt{5}-1}{2}$ ,  $\omega_2 = s^{-1}$ ,  $\lambda_1 = \lambda_2 = 0.8$ ,  $\gamma = 0.01$ . Left panel: Plots of  $\varepsilon$  vs  $\|K_1\|_{2,\parallel}$ ,  $\varepsilon$  vs  $\|K_2\|_{2,\parallel}$ ,  $\varepsilon$  vs  $\|K_1\|_{2,\perp}$ ,  $\varepsilon$  vs  $\|K_2\|_{2,\perp}$ ; using the data in Table 5. Right panel: poles of Padé and log-Padé approximants for  $N = 256$ .

by the fact that periodic orbits exist for a whole interval of the parameters, the so-called *Arnold tongues* ([3]). Besides, in the conservative case one can take advantage of the existence of symmetry lines to ease the search of periodic orbits; symmetry lines do not



exist in the dissipative case. Furthermore, the application of Greene's method to higher dimensional systems (like the 4-dim standard map) is not trivial, since the search for the approximating periodic orbits might be computationally difficult, as shown for example in [15]. In the rest of this Section, we implement a numerical method that allows us to apply Greene's method also in the 4-dim case, although we are aware of the fact that it is computationally expensive and less accurate than Lindstedt series expansion and Sobolev's criterion.

Let us write (11) as the map  $\underline{f} : \mathbb{R}^2 \times \mathbb{T}^2 \rightarrow \mathbb{R}^2 \times \mathbb{T}^2$ , given by

$$\begin{aligned} y' &= \lambda y + \mu + \varepsilon(V(x) + \gamma Q(x, z)) \\ x' &= x + y' \\ w' &= w + \varepsilon(V(z) - \gamma Q(x, z)) \\ z' &= z + w' \end{aligned} \tag{57}$$

with  $0 < \lambda < 1$ ,  $\mu \in \mathbb{R}$ ,  $\varepsilon \in \mathbb{R}_+$ ,  $\gamma \in \mathbb{R}$ . In the following, we will consider the functions

$$V(x) := \sin(x) , \quad Q(x, z) := \sin(x - z) . \tag{58}$$

Let  $\tilde{\underline{f}} : \mathbb{R}^4 \rightarrow \mathbb{R}^4$  be the lift of  $\underline{f}$  and let  $\underline{\omega} = (\frac{p_1}{q}, \frac{p_2}{q})$  be the frequency vector with  $p_1, p_2 \in \mathbb{Z}$ ,  $q \in \mathbb{Z} \setminus \{0\}$ . A periodic orbit with frequency  $\underline{\omega}$  satisfies the condition

$$\tilde{\underline{f}}^q(\underline{X}) = \underline{X} + (0, 2\pi p_1, 0, 2\pi p_2)$$

for  $\underline{X} = (y, x, w, z)$ . Searching for periodic orbits is equivalent to find the roots of the function

$$\underline{G}(\underline{X}) := \tilde{\underline{f}}^q(\underline{X}) - \underline{X} - (0, 2\pi p_1, 0, 2\pi p_2) . \tag{59}$$

Following (12), we recall that the frequency can be computed as

$$\underline{\omega} = \left( \lim_{n \rightarrow \infty} \frac{x_n - x_0}{n} , \lim_{n \rightarrow \infty} \frac{z_n - z_0}{n} \right) , \tag{60}$$

where the subscript denotes the  $n$ -th iterate.

To solve (59), we need a good initial guess. To this end, we consider (57) with  $\gamma = 0$ , so that we obtain two uncoupled systems (a conservative and a dissipative 2-dim standard maps). Let us denote the dissipative map for  $\gamma = 0$  as  $\underline{M}_d : \mathbb{R} \times \mathbb{T} \rightarrow \mathbb{R} \times \mathbb{T}$ , defined as

$$\begin{aligned} y' &= \lambda y + \mu + \varepsilon \sin(x) \\ x' &= x + y' . \end{aligned} \tag{61}$$

For a fixed  $\lambda$ , we look for  $(y_0, x_0, \mu)$  such that  $\underline{M}_d$  admits a periodic orbit with period  $2\pi\frac{p_1}{q}$ . From (59) with  $\gamma = 0$  we need to solve the condition

$$(y_0, x_0) = \widetilde{\underline{M}}_d^q(y_0, x_0; \mu) - (0, 2\pi p_1) , \quad (62)$$

where  $\widetilde{\underline{M}}_d : \mathbb{R}^2 \rightarrow \mathbb{R}^2$  denotes the lift of  $\underline{M}_d$ . Since we aim to find three unknowns  $(y_0, x_0, \mu)$  that solve (62), the system is clearly underdetermined. To overcome this problem, we implemented the following procedure, which we have heuristically found and which turns out to be useful for our purposes.

Let us introduce  $\mu' \in \mathbb{R}$  as  $\mu' = y'(1 - \lambda) - \varepsilon \sin(x')$ , which is not constant as  $(y', x')$  vary. However, for any  $(y_0, x_0)$  that fulfills (62), we may seek for a value of  $\mu = \mu_0$  such that  $\mu_0 = \mu_q$ . This observation leads us to define the mapping  $\widetilde{\underline{M}}_e : \mathbb{R}^3 \rightarrow \mathbb{R}^3$  as an extension of  $\underline{M}_d$  as follows:

$$\begin{aligned} y' &= \lambda y + \mu + \varepsilon \sin(x) \\ x' &= x + y' \\ \mu' &= y'(1 - \lambda) - \varepsilon \sin(x') . \end{aligned} \quad (63)$$

Any triple  $(y_0, x_0, \mu_0)$  that fulfills

$$(y_0, x_0, \mu_0) = \widetilde{\underline{M}}_e^q(y_0, x_0, \mu_0) - (0, 2\pi p_1, 0) \quad (64)$$

provides a  $2\pi p_1/q$  periodic orbit of the original dissipative mapping (61). We further validate the result by checking that the frequency associated to the solution  $(y_0, x_0, \mu_0)$  coincides with the first component of  $\underline{\omega}$  in (60).

Concerning the symplectic case for  $\gamma = 0$ , let us denote the conservative map as  $\underline{M}_c : \mathbb{R} \times \mathbb{T} \rightarrow \mathbb{R} \times \mathbb{T}$ , defined by the equations

$$\begin{aligned} w' &= w + \varepsilon \sin(z) \\ z' &= z + w' . \end{aligned} \quad (65)$$

To get a periodic orbit with frequency equal to  $2\pi p_2/q$ , we need to solve

$$(w_0, z_0) = \widetilde{\underline{M}}_c^q(w_0, z_0) - (0, 2\pi p_2) , \quad (66)$$

where we have introduced the lift  $\widetilde{\underline{M}}_c : \mathbb{R}^2 \rightarrow \mathbb{R}^2$ . The solution of (64) and (66) provides an initial guess for  $\gamma = 0$ .

We show two examples of stable periodic orbits in Fig. 9 for the dissipative standard map with  $\lambda = 0.8$ ; the left panel refers to the approximant 610/987 to  $\varpi$  and the right panel refers to the approximant 619/820 to  $s^{-1}$ .

TABLE 6. Parameters and initial conditions for stable periodic orbits of the map (61) with  $\lambda = 0.8$ , and for approximants to the frequencies  $\omega_1 = \varpi$  (top) and  $\omega_1 = s^{-1}$  (bottom).

$p$	$q$	$\varepsilon_c$	$y$	$x$	$\mu$
2	3	1.384	3.85392	3.18291	0.82796
3	5	1.185	3.64736	3.15981	0.75105
5	8	1.123	4.38290	0.08371	0.78265
8	13	1.028	3.71189	3.16654	0.76804
13	21	1.004	3.72204	3.16861	0.77153
21	34	0.992	3.72107	3.16802	0.77043
34	55	0.984	3.72286	3.16834	0.77090
55	89	0.970	4.22374	0.07620	0.77090
89	144	0.946	4.21299	0.07552	0.77121
144	233	0.945	4.21273	0.07551	0.77119
233	377	0.975	4.22626	0.07635	0.77088
377	610	0.976	4.22709	0.07640	0.77086
610	987	0.973	4.22564	0.07631	0.77089
$p$	$q$	$\varepsilon_c$	$y$	$x$	$\mu$
3	4	1.156	5.260275	0.110313	0.924791
37	49	0.787	5.233906	0.141309	0.935855
40	53	0.779	5.225298	0.140582	0.935884
77	102	0.774	5.220786	0.140221	0.935981
271	359	0.753	4.370078	3.224267	0.936199
619	820	0.758	5.206642	0.139073	0.936139

The critical values  $\varepsilon_c$  in Table 6 are the maximum values of the parameter for which the periodic orbit is stable; they have been obtained by solving (64), increasing  $\varepsilon$  until the linear stability of the orbit is lost.

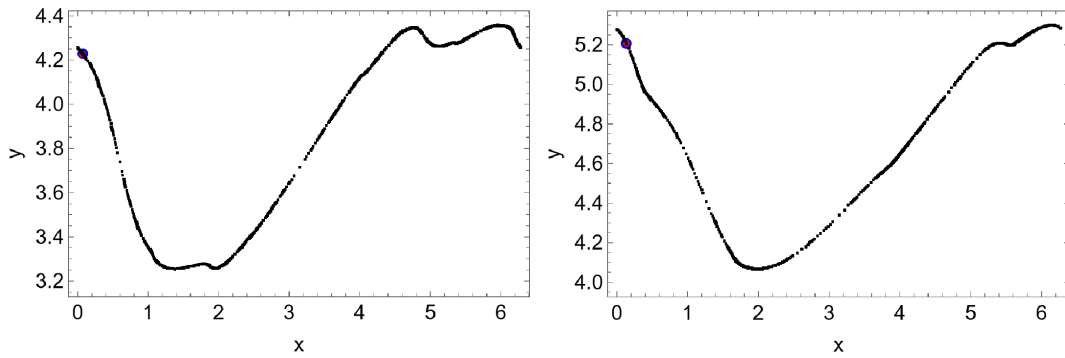


FIGURE 9. Stable periodic orbit of the map (61) with  $V(x) = \sin(x)$  with  $\omega_1 = 610/987$  (left) and  $\omega_1 = 619/820$  (right). For parameters and initial conditions, see Tab. 6 (initial condition indicated by a red point).

We notice that the linear stability is calculated by computing the eigenvalues  $\kappa_1, \kappa_2$  of the product of the Jacobian of the map over the periodic orbit (see Appendix C). If  $\max(|\kappa_1|, |\kappa_2|) > 1$  the orbit is said to be unstable.

In the 4-dim case, we proceed as follows. We assume to have a starting point given by

$$\underline{X}_0 := (y_0, x_0, w_0, z_0) ,$$

so that for  $\gamma = 0$  we obtain a periodic orbit for  $\underline{M}_d$  with period  $\frac{p_1}{q}$  starting from  $(y_0, x_0)$  and a periodic orbit for  $\underline{M}_c$  with period  $\frac{p_2}{q}$  starting from  $(w_0, z_0)$ <sup>1</sup>. We apply a continuation method in  $\varepsilon$  and at each step we require to solve (64) and (66) to obtain  $(y_0, x_0, \mu_0)$  and  $(w_0, z_0)$ , respectively, as an initial guess to solve (59). However, since the solution  $\underline{X}^{(\gamma)} = (y^{(\gamma)}, x^{(\gamma)}, w^{(\gamma)}, z^{(\gamma)})$  for  $\gamma \neq 0$  requires to adapt  $(y_0, x_0, \mu_0)$ , as well as  $(w_0, z_0)$  simultaneously at each step of the continuation method, we are led to solve the system of equations

$$\begin{aligned} y^{(\gamma)} &= \tilde{f}_1^q(\underline{X}^{(\gamma)}, \mu^{(\gamma)}) & x^{(\gamma)} &= \tilde{f}_2^q(\underline{X}^{(\gamma)}, \mu^{(\gamma)}) - 2\pi p_1 \\ w^{(\gamma)} &= \tilde{f}_3^q(\underline{X}^{(\gamma)}, \mu^{(\gamma)}) & z^{(\gamma)} &= \tilde{f}_4^q(\underline{X}^{(\gamma)}, \mu^{(\gamma)}) - 2\pi p_2 \\ \mu^{(\gamma)} &= \tilde{f}_e^q(\underline{X}^{(\gamma)}, \mu^{(\gamma)}) \end{aligned}$$

with respect to  $\underline{X}^{(\gamma)}$  and  $\mu^{(\gamma)}$  in the vicinity of  $(\underline{X}^{(0)}, \mu^{(0)})$ , having defined

$$\tilde{f}_e := \lambda(y - 1) - \varepsilon(V(x) + \gamma Q(x, z)) .$$

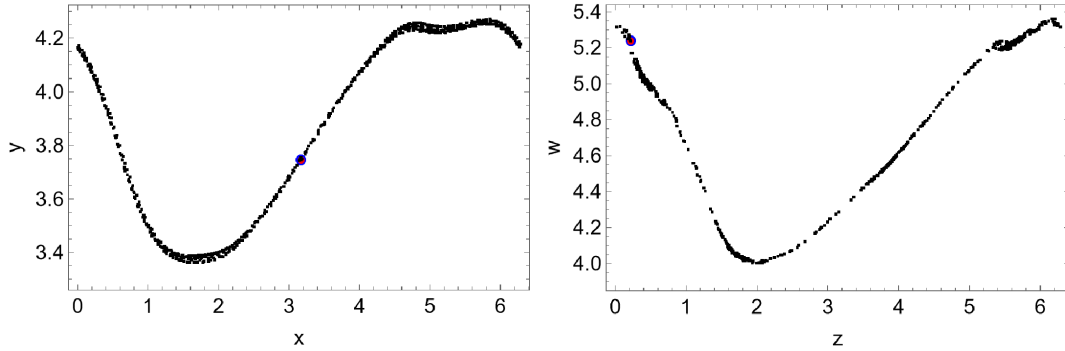


FIGURE 10. Stable periodic orbit of the map (67) with  $V(x) = \sin(x)$ ,  $Q(x, y) = \sin(x - z)$  and using  $\varepsilon = 0.783$   $\gamma = 0.01$ ,  $\lambda_1 = 0.8$ ,  $\lambda_2 = 0.7$  with  $p_1 = 411$ ,  $p_2 = 502$ ,  $q = 665$ . Initial conditions in blue and state after  $q$  iterations in red.

<sup>1</sup>Computationally expensive means that: (i) the root finding method might need a large number of iterations to converge to the requested accuracy; (ii) the computations require accuracy, which means even more than 1000 digits in the iteration of the mapping; (iii) if the root finding fails, one needs to find better initial conditions which is highly non trivial; (iv) the continuation method only works with a small step for the perturbing parameter.

Let us now consider the generalization of the dissipative 4-dim map (57):

$$\begin{aligned}
y' &= \lambda_1 y + \mu_1 + \varepsilon(V(x) + \gamma Q(x, z)) \\
x' &= x + y' \\
w' &= \lambda_2 w + \mu_2 + \varepsilon(V(z) - \gamma Q(x, z)) \\
z' &= z + w'
\end{aligned} \tag{67}$$

with  $0 < \lambda_{1,2} \leq 1$ ,  $\mu_{1,2} \in \mathbb{R}$  and  $V, Q, \varepsilon, \gamma$  as in (57). Using the same approach outlined for the mixed case, we introduce the extension of (67) through the following additional mapping equations:

$$\begin{aligned}
\mu'_1 &= \lambda_1(y' - 1) - \varepsilon(V(x') + \gamma Q(x', z')) \\
\mu'_2 &= \lambda_2(w' - 1) - \varepsilon(V(z') - \gamma Q(x', z')) .
\end{aligned} \tag{68}$$

Any  $2\pi p_1/q$ ,  $2\pi p_2/q$  periodic orbit of (67) needs to fulfill the conditions  $y_q^{(\gamma)} = y_0$ ,  $x_q^{(\gamma)} = x_0$ ,  $z_q^{(\gamma)} = z_0 + 2\pi p_1$ ,  $w_q^{(\gamma)} = w_0 + 2\pi p_2$  with  $\mu_{1,0}^{(\gamma)} = \mu_{1,0}$ ,  $\mu_{2,0}^{(\gamma)} = \mu_{2,0}$ . Hence, we are led to solve the system of equations:

$$\begin{aligned}
y^{(\gamma)} &= \tilde{f}_1^q(\underline{X}^{(\gamma)}, \underline{\mu}^{(\gamma)}) & x^{(\gamma)} &= \tilde{f}_2^q(\underline{X}^{(\gamma)}, \underline{\mu}^{(\gamma)}) - 2\pi p_1 \\
w^{(\gamma)} &= \tilde{f}_3^q(\underline{X}^{(\gamma)}, \underline{\mu}^{(\gamma)}) & z^{(\gamma)} &= \tilde{f}_4^q(\underline{X}^{(\gamma)}, \underline{\mu}^{(\gamma)}) - 2\pi p_2 \\
\mu_1^{(\gamma)} &= \tilde{f}_{1e}^q(\underline{X}^{(\gamma)}, \mu_1^{(\gamma)}) & \mu_2^{(\gamma)} &= \tilde{f}_{3e}^q(\underline{X}^{(\gamma)}, \mu_2^{(\gamma)})
\end{aligned} \tag{69}$$

with  $\underline{X}^{(\gamma)} = (y^{(\gamma)}, x^{(\gamma)}, w^{(\gamma)}, z^{(\gamma)})$ ,  $\underline{\mu}^{(\gamma)} = (\mu_1^{(\gamma)}, \mu_2^{(\gamma)})$ , having defined the functions

$$\begin{aligned}
\tilde{f}_{1,e} &:= \lambda_1(y - 1) - \varepsilon(V(x) + \gamma Q(x, z)) \\
\tilde{f}_{2,e} &:= \lambda_2(w - 1) - \varepsilon(V(z) - \gamma Q(x, z)) .
\end{aligned} \tag{70}$$

Fixing  $p_1, p_2, q$  and the parameters  $\lambda_1, \lambda_2, \varepsilon, \gamma$ , we solve the equations (69) and (70) for  $\underline{X}^{(\gamma)}, \underline{\mu}^{(\gamma)}$ , and use  $\mu_1 = \mu_1^{(\gamma)}, \mu_2 = \mu_2^{(\gamma)}$ , together with the above parameters and initial conditions  $\underline{X}^{(\gamma)}$  to iterate (67). An example is shown in Figure 10 with initial conditions and parameters detailed in Table 7, which provides the results for several approximants to  $\varpi$  and  $s^{-1}$ . Linear stability is granted provided all eigenvalues lie within the unit circle, which is true for the orbit shown in Figure 10.

The threshold  $\varepsilon$  is obtained according to Greene's approach: for a given triple  $(p_1, p_2, q)$ , having fixed  $\varepsilon, \gamma, \lambda_1, \lambda_2$ , we numerically solve (69) in the unknowns  $\underline{x}^{(\gamma)}$  and  $\underline{\mu}^{(\gamma)}$ . By a continuation method, we increase  $\varepsilon$  until the maximum of the absolute values of the real parts of the eigenvalues of the product matrix of the Jacobian associated to a given periodic orbit crosses one from below.

TABLE 7. Parameters and initial conditions for the periodic orbits approximating  $\omega_1 = p_1/q$  and  $\omega_2 = p_2/q$  for  $\gamma = 0.01$ ,  $\lambda_1 = 0.8$ ,  $\lambda_2 = 0.7$ . Values are provided close to breakdown threshold in  $\varepsilon$ , where the orbits are still linearly stable and just before they become unstable (u).

	$p_1$	$p_2$	$q$	$\varepsilon$	$y$	$x$	$w$	$z$	$\mu_1$	$\mu_2$
1	4	5	6	u	4.2205	0.0627	5.140	3.420	0.8376	1.5692
2	4	5	7	0.578	3.5551	3.1540	4.750	0.158	0.7174	1.3357
3	5	6	8	1.000	3.7446	3.1704	4.200	3.260	0.7787	1.3816
4	18	22	29	0.500	4.0498	0.0648	5.050	0.196	0.7782	1.4167
5	63	77	102	0.794	4.1539	0.0750	5.200	0.199	0.7722	1.3997
6	131	160	212	0.775	4.1328	0.0689	4.340	3.270	0.7727	1.3999
7	411	502	665	0.783	3.7437	3.1742	5.240	0.222	0.7728	1.3998

The evolution of the maxima with respect to  $\varepsilon$  for the triples  $(p_1, p_2, q)$  in Table 7 is shown in Figure 11. We have been able to find periodic orbits up to  $(p_1, p_2, q) = (411, 502, 665)$  for which we obtain that the orbit is stable up to  $\varepsilon = 0.783$ . We can take this value as a lower bound estimate on the breakdown threshold of the invariant torus, which is consistent with the outer circle bounding the domain of the Padé approximants of Figure 5.

We conclude by noticing that in all cases the threshold in  $\varepsilon$  is reached as follows. When approaching the threshold, the maximum of the eigenvalues of a given periodic orbit starts to experience wild oscillations, also below one, ending up in a jump above one, possibly reaching high values that denote a sharp instability of the periodic orbit (compare with the right panel of Figure 11).

**Acknowledgements.** We are grateful to Rafael de la Llave for many discussions and suggestions, which helped us to improve this work.

## APPENDIX A. PADÉ APPROXIMANTS

The analyticity domains of the Lindstedt series expansions of Section 6 can be obtained through the computation of the Padé approximants, that we briefly recall as follows, referring to [4] for further details.

Given the series

$$W(\varepsilon) = \sum_{k=1}^{\infty} W_k \varepsilon^k ,$$

we define the Padé approximants to  $W$  of order  $[M, N]$  for  $M, N \in \mathbb{N}$  as the functions  $\mathcal{P}_{M,N}(\varepsilon)$ , which are the ratio of the polynomials  $P^{(M)}(\varepsilon)$ ,  $Q^{(N)}(\varepsilon)$  of degree, respectively,

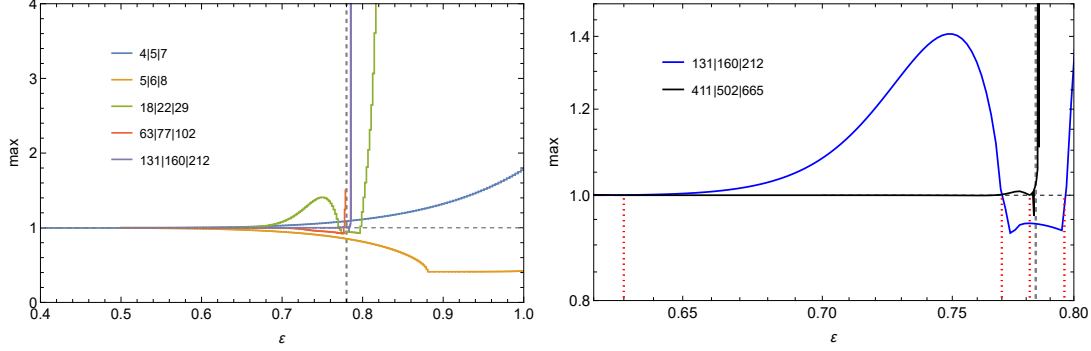


FIGURE 11. Maximum absolute real part of the eigenvalues of the product of the Jacobian matrices along the  $p_1/q$  and  $p_2/q$  periodic orbits with increasing  $\varepsilon$  and  $\gamma = 0.01$ ,  $\lambda_1 = 0.8$ ,  $\lambda_2 = 0.7$ . Left: the vertical dashed line indicates the lower threshold bound  $\varepsilon = 0.783$ . Right: zoom for the two periodic orbits with frequencies  $(p_1, p_2, q) = (131, 160, 212)$  - blue line - and  $(p_1, p_2, q) = (411, 502, 665)$  - black line. The vertical dashed line corresponds to  $\varepsilon = 0.783$ .

$M$  and  $N$ , say

$$\mathcal{P}_{M,N}(\varepsilon) := \frac{P^{(M)}(\varepsilon)}{Q^{(N)}(\varepsilon)} ,$$

such that the Taylor expansion of  $\mathcal{P}_{M,N}(\varepsilon)$  coincides with the Taylor expansion of  $W$  up to order  $M + N$ :

$$W(\varepsilon)Q^{(N)}(\varepsilon) - P^{(M)}(\varepsilon) = O(\varepsilon^{M+N+1}) .$$

We can expand  $P_M$  and  $Q_N$  as

$$P^{(M)}(\varepsilon) = \sum_{j=0}^M P_j \varepsilon^j , \quad Q^{(N)}(\varepsilon) = \sum_{j=0}^N Q_j \varepsilon^j .$$

Then, the function  $\mathcal{P}_{M,N}(\varepsilon)$  contains  $M + N + 1$  unknown coefficients, since we can normalize  $Q_0 = 1$ .

The coefficients  $P_j$ ,  $Q_j$  can be computed through the following recursive formulae:

$$\begin{aligned} W_i + \sum_{j=1}^N W_{i-j} Q_j &= 0 , \quad M < i \leq M + N , \\ W_i + \sum_{j=1}^i W_{i-j} Q_j &= P_i , \quad 0 \leq i \leq M , \end{aligned}$$

where the first equation gives  $Q_j$  and the second equation gives  $P_j$ .

The analyticity domain of the function  $W$  can then be obtained by computing the zeros of  $Q_N$ . Typically, one considers diagonal Padé approximants of order  $[N, N]$ . It is

often necessary to eliminate fake zeros, which can be distinguished from genuine ones for the fact that fake zeros disappear when the order of the Padé approximants changes or when the parameters are slightly changed ([6]).

## APPENDIX B. ALGORITHM OF THE NEWTON STEP

In the algorithm below for the Newton step, we use the following notation:  $\overline{B}$  means the average of  $B$ , while  $(B)^o$  denotes the zero average part, namely  $(B)^o = B - \overline{B}$ .

**Algorithm 13.** *Given  $\underline{K} : \mathbb{T}^2 \rightarrow \mathbb{T}^2 \times \mathbb{R}^2$ ,  $\underline{\mu} \in \mathbb{R}^2$ , we perform the following computations:*

- 1)  $\underline{E} \leftarrow \underline{f}_{\underline{\mu}, \varepsilon} \circ \underline{K} - \underline{K} \circ T_{\underline{\omega}}$
- 2)  $\underline{\alpha} \leftarrow D\underline{K}$
- 3)  $N \leftarrow [\underline{\alpha}^\top \underline{\alpha}]^{-1}$
- 4)  $M \leftarrow [\underline{\alpha}, J^{-1} \underline{\alpha} N]$
- 5)  $\beta \leftarrow M^{-1} \circ T_{\underline{\omega}}$
- 6)  $\tilde{E} \leftarrow \beta \underline{E}$
- 7)  $P \leftarrow \underline{\alpha} N$   
 $\gamma \leftarrow \underline{\alpha}^\top J^{-1} \underline{\alpha}$   
 $S \leftarrow (P \circ T_{\underline{\omega}})^\top D\underline{f}_{\underline{\mu}, \varepsilon} \circ \underline{K} J^{-1} P - \lambda (N \circ T_{\underline{\omega}})^\top (\gamma \circ T_{\underline{\omega}}) (N \circ T_{\underline{\omega}})$   
 $\tilde{A} \leftarrow M^{-1} \circ T_{\underline{\omega}} D_{\underline{\mu}} \underline{f}_{\underline{\mu}, \varepsilon} \circ \underline{K}$
- 8)  $(\underline{Ba})^0$  solves  $\lambda(\underline{Ba})^0 - (\underline{Ba})^0 \circ T_{\underline{\omega}} = -(\tilde{E}_2)^0$   
 $(\underline{Bb})^0$  solves  $\lambda(\underline{Bb})^0 - (\underline{Bb})^0 \circ T_{\underline{\omega}} = -(\tilde{A}_2)^0$
- 9) Find  $\overline{W}_2, \underline{\sigma}$  solving

$$\begin{pmatrix} \overline{S} & \overline{S(\underline{Bb})^0} + \overline{\tilde{A}_1} \\ (\lambda - 1)Id & \overline{\tilde{A}_2} \end{pmatrix} \begin{pmatrix} \overline{W}_2 \\ \underline{\sigma} \end{pmatrix} = \begin{pmatrix} -\overline{\tilde{E}_1} - \overline{S(\underline{Ba})^0} \\ -\overline{\tilde{E}_2} \end{pmatrix}$$

- 10)  $(\underline{W}_2)^0 = (\underline{Ba})^0 + (\underline{Bb})^0 \underline{\sigma}$
- 11)  $\underline{W}_2 = (\underline{W}_2)^0 + \overline{W}_2$
- 12)  $(\underline{W}_1)^0$  solves  $(\underline{W}_1)^0 - (\underline{W}_1)^0 \circ T_{\underline{\omega}} = -(\underline{SW}_2)^0 - (\tilde{E}_1)^0 - (\tilde{A}_1)^0 \underline{\sigma}$
- 13)  $\underline{K} \leftarrow \underline{K} + M \underline{W}$   
 $\underline{\mu} \leftarrow \underline{\mu} + \underline{\sigma}$ .



## APPENDIX C. LINEAR STABILITY

Let  $\underline{f} : \mathbb{R}^4 \rightarrow \mathbb{R}^4$  be a vector-valued function with components  $\underline{f} = (f_1, \dots, f_4)$  and let  $\underline{x} = (x_1, \dots, x_4) \in \mathbb{R}^4$ . We denote by  $J_f$  the Jacobian defined as

$$J_f = \begin{pmatrix} \frac{\partial f_1}{\partial x_1} & \cdots & \frac{\partial f_1}{\partial x_4} \\ \vdots & \dots & \vdots \\ \frac{\partial f_4}{\partial x_1} & \cdots & \frac{\partial f_4}{\partial x_4} \end{pmatrix}.$$

For the map (67), using (58), the matrix  $J_f$  becomes

$$J_f = \begin{pmatrix} \lambda_1 & \varepsilon (\cos(x_2) + \gamma \cos(x_2 - x_4)) & 0 & -\varepsilon \gamma \cos(x_2 - x_4) \\ \lambda_1 & 1 + \varepsilon (\cos(x_2) + \gamma \cos(x_2 - x_4)) & 0 & -\varepsilon \gamma (\cos(x_2 - x_4)) \\ 0 & -\varepsilon \gamma \cos(x_2 - x_4) & \lambda_2 & \varepsilon (\cos(x_4) + \gamma \cos(x_2 - x_4)) \\ 0 & -\varepsilon \gamma \cos(x_2 - x_4) & \lambda_2 & 1 + \varepsilon (\cos(x_4) + \gamma \cos(x_2 - x_4)) \end{pmatrix}$$

(notice that, with reference to (67), we used the following notation:  $x_1 = y$ ,  $x_2 = x$ ,  $x_3 = w$ ,  $x_4 = z$ ). We remark that the same expression for  $J_f$  can be used for (57) by setting  $\lambda_2 = 1$ , the upper right  $2 \times 2$  sub-matrix can be used to obtain  $J_f$  for (61) by setting  $\lambda_1 = \lambda$ ,  $\gamma = 0$ , and the lower right  $2 \times 2$  sub-matrix is equivalent to  $J_f$  for (65) by setting  $\lambda_2 = 1$  and  $\gamma = 0$ .

Let  $\underline{x}_n = \underline{f}(\underline{x}_{n-1})$  be the  $n$ -th iteration starting from  $\underline{x} = \underline{x}_0$  with  $\underline{x}_0 = (x_{1,0}, \dots, x_{m,0})$  and let  $\underline{x}_q$  be the  $q$ -periodic orbit such that

$$\underline{x}_q = (x_{1,0}, x_{2,0} + 2\pi p_1, x_{3,0}, x_{4,0} + 2\pi p_2)$$

with  $p_1, p_2, q \in \mathbb{Z}_+$ ,  $q \neq 0$ . We denote by  $J_T$  the product of the Jacobian matrices  $J_f$  evaluated along the orbit  $\underline{x}_q$ :

$$J_T = \prod_{k=0}^{q-1} J_f|_{\underline{x}=\underline{x}_k}.$$

The linear stability of  $\underline{x}_q$  is determined by computing the real parts of the eigenvalues  $\kappa_1, \dots, \kappa_4$  of the matrix  $J_T$ . A  $(p_1, p_2, q)$ -periodic orbit is called *linearly stable*, if all of the eigenvalues lie within the unit circle, i.e.

$$\max_{k=1, \dots, 4} \operatorname{Re}(\kappa_k) \leq 1. \quad (71)$$

If the condition (71) is violated, we say that the orbit is unstable.

## REFERENCES

- [1] V. Arnold. Instability of dynamical systems with several degrees of freedom. *Sov. Math. Doklady*, 5:581–585, 1964.
- [2] V. I. Arnol'd. Proof of a theorem of A. N. Kolmogorov on the invariance of quasi-periodic motions under small perturbations. *Russian Math. Surveys*, 18(5):9–36, 1963.

- [3] V. I. Arnol'd. Small denominators. i. mappings of the circumference onto itself. *Amer. Math. Soc. Transl. Ser. 2*, 46:213–284, 1965. English translation: *Amer. Math. Soc. Transl. (2)*, 46:213–284, 1965.
- [4] G. A. Baker, G. A. Baker Jr, P. Graves-Morris, G. Baker, and S. S. Baker. *Padé Approximants: Encyclopedia of Mathematics and It's Applications, Vol. 59 George A. Baker, Jr., Peter Graves-Morris*, volume 59. Cambridge University Press, 1996.
- [5] A. Berretti, A. Celletti, L. Chierchia, and C. Falcolini. Natural boundaries for area-preserving twist maps. *J. Statist. Phys.*, 66(5-6):1613–1630, 1992.
- [6] A. Berretti, A. Celletti, L. Chierchia, and C. Falcolini. Natural boundaries for area-preserving twist maps. *J. Statist. Phys.*, 66(5-6):1613–1630, 1992.
- [7] T. Blass and R. de la Llave. The analyticity breakdown for Frenkel-Kontorova models in quasi-periodic media: numerical explorations. *J. Stat. Phys.*, 150(6):1183–1200, 2013.
- [8] A. P. Bustamante and R. C. Calleja. Computation of domains of analyticity for the dissipative standard map in the limit of small dissipation. *Phys. D*, 395:15–23, 2019.
- [9] A. P. Bustamante and R. C. Calleja. Corrigendum and addendum to “Computation of domains of analyticity for the dissipative standard map in the limit of small dissipation” [Physica D 395 (2019) 15–23]. *Phys. D*, 417:Paper No. 132837, 7, 2021.
- [10] R. Calleja and A. Celletti. Breakdown of invariant attractors for the dissipative standard map. *CHAOS*, 20(1):013121, 2010.
- [11] R. Calleja, A. Celletti, J. Gimeno, and R. de la Llave. KAM quasi-periodic tori for the dissipative spin-orbit problem. *Commun. Nonlinear Sci. Numer. Simul.*, 106:Paper No. 106099, 22, 2022.
- [12] R. C. Calleja. *Existence and persistence of invariant objects in dynamical systems and mathematical physics*. Ph.D. thesis, The University of Texas at Austin, 2009.
- [13] R. C. Calleja, A. Celletti, and R. de la Llave. A KAM theory for conformally symplectic systems: efficient algorithms and their validation. *J. Differential Equations*, 255(5):978–1049, 2013.
- [14] R. C. Calleja, A. Celletti, J. Gimeno, and R. de la Llave. A map reduction and KAM tori construction for the dissipative spin-orbit problem. *Preprint*, 2020.
- [15] R. C. Calleja, A. Celletti, J. Gimeno, and R. de la Llave. Accurate computations up to break-down of quasi-periodic attractors in the dissipative spin-orbit problem. *Preprint*, 2022.
- [16] A. Celletti. *Stability and Chaos in Celestial Mechanics*. Springer-Verlag, Berlin; published in association with Praxis Publishing, Chichester, 2010.
- [17] A. Celletti and L. Chierchia. A constructive theory of Lagrangian tori and computer-assisted applications. In *Dynamics Reported*, pages 60–129. Springer, Berlin, 1995.
- [18] B. Chirikov. A universal instability of many-dimensional oscillator systems. *Phys. Rep.*, 52(5):264–379, 1979.
- [19] R. de la Llave, A. González, À. Jorba, and J. Villanueva. KAM theory without action-angle variables. *Nonlinearity*, 18(2):855–895, 2005.
- [20] R. de La Llave and S. Tompaidis. Nature of singularities for analyticity domains of invariant curves. *Physical Review Letters*, 73(11):1459, 1994.
- [21] R. De La Llave and S. Tompaidis. On the singularity structure of invariant curves of symplectic mappings. *Chaos: An Interdisciplinary Journal of Nonlinear Science*, 5(1):227–237, 1995.
- [22] R. Dvorak and C. Lhotka. *Celestial Dynamics: Chaoticity and Dynamics of Celestial Systems*. Wiley, 2013.
- [23] A. M. Fox and J. D. Meiss. Greene’s residue criterion for the breakup of invariant tori of volume-preserving maps. *Phys. D*, 243:45–63, 2013.
- [24] J. M. Greene. A method for determining a stochastic transition. *Jour. Math. Phys.*, 20:1183–1201, 1979.
- [25] A. Haro, M. Canadell, J.-L. Figueras, A. Luque, and J.-M. Mondelo. *The parameterization method for invariant manifolds*, volume 195 of *Applied Mathematical Sciences*. Springer, [Cham], 2016. From rigorous results to effective computations.
- [26] Y. A. Khinchin. Continued fractions. *Dover Publications*, 1997.

- [27] S.-H. Kim and S. Östlund. Simultaneous rational approximations in the study of dynamical systems. *Phys. Rev. A (3)*, 34(4):3426–3434, 1986.
- [28] A. N. Kolmogorov. On conservation of conditionally periodic motions for a small change in Hamilton’s function. *Dokl. Akad. Nauk SSSR (N.S.)*, 98:527–530, 1954. English translation in *Stochastic Behavior in Classical and Quantum Hamiltonian Systems (Volta Memorial Conf., Como, 1977)*, Lecture Notes in Phys., 93, pages 51–56. Springer, Berlin, 1979.
- [29] J. D. Meiss and E. Sander. Birkhoff averages and the breakdown of invariant tori in volume-preserving maps. *Phys. D*, 428:Paper No. 133048, 20, 2021.
- [30] J. Moser. On invariant curves of area-preserving mappings of an annulus. *Nachr. Akad. Wiss. Göttingen Math.-Phys. Kl. II*, 1962:1–20, 1962.
- [31] H. Poincaré. *Les méthodes nouvelles de la mécanique céleste*, volume 1, 2, 3. Gauthier-Villars, Paris, 1892–1899.
- [32] F. Schweiger. On the invariant measure for Jacobi-Perron algorithm. *Math. Pannon.*, 1(2):91–106, 1990.
- [33] S. Tompaids. Approximation of invariant surfaces by periodic orbits in high-dimensional maps: some rigorous results. *Experiment. Math.*, 5(3):197–209, 1996.
- [34] S. Tompaids. Numerical study of invariant sets of a quasiperiodic perturbation of a symplectic map. *Experiment. Math.*, 5(3):211–230, 1996.

DEPARTMENT OF MATHEMATICS, UNIVERSITY OF ROMA TOR VERGATA, VIA DELLA RICERCA SCIENTIFICA 1, 00133 ROMA (ITALY)

*Email address:* bustamante@mat.uniroma2.it

DEPARTMENT OF MATHEMATICS, UNIVERSITY OF ROMA TOR VERGATA, VIA DELLA RICERCA SCIENTIFICA 1, 00133 ROMA (ITALY)

*Email address:* celletti@mat.uniroma2.it

DEPARTMENT OF MATHEMATICS, UNIVERSITY OF ROMA TOR VERGATA, VIA DELLA RICERCA SCIENTIFICA 1, 00133 ROMA (ITALY)

*Email address:* lhotka@mat.uniroma2.it